Pergamon

Geochimica et Cosmochimica Acta, Vol. 65, No. 2, pp. 323–342, 2001

0016-7037/01 $20.00 + .00

PII S0016-7037(00)00516-0

The Portales Valley meteorite breccia: Evidence for impact-induced melting and metamorphism of an ordinary chondrite

ALAN E. RUBIN,[1,*] FINN ULFF-MØLLER,[1] JOHN T. WASSON,[1,2] and WILLIAM D. CARLSON[3]

[1]Institute of Geophysics and Planetary Physics, University of California, Los Angeles, California 90095-1567, USA
[2]Department of Chemistry and Biochemistry and Department of Earth and Space Sciences, University of California, Los Angeles, California 90095, USA
[3]Department of Geological Sciences, University of Texas at Austin, Austin, Texas 78712-1101, USA

(*Received July* 21, 1999; *accepted in revised form July* 24, 2000)

Abstract—The Portales Valley H-chondrite fall is an annealed impact-melt breccia with coarse metal interstitial to angular and subrounded silicate clasts. The large metal-rich regions exhibit a Widmanstätten structure and contain very little troilite. We were able to examine a 16.5 kg metal-rich specimen of Portales Valley. Silicates contain numerous flecks of metallic Cu and curvilinear trails of tiny metallic Fe–Ni blebs, characteristic of shocked and annealed chondrites. One silicate clast appears to have experienced little (<10%) or no melting; it is essentially identical to normal H6 chondrites. Other clasts are finer grained and have a low abundance of recognizable relict chondrules; they are significantly enriched in troilite and depleted in metallic Fe–Ni relative to typical H chondrites. Their low metal abundance indicates that they are not simply ultra-recrystallized H6 chondrites. If the silicates in these clasts started off as normal H-chondrite material and were recrystallized to the same extent as the progenitor of the H6-like clast, then their low modal abundance of chondrules indicates that they experienced significant crushing and/or impact melting. We infer that most of the metal and troilite was lost from these silicate clasts during impact melting; it appears that troilite was reintroduced into the silicates, perhaps by an S_2-rich vapor (that formed FeS by reacting with Fe vapor or residual metal). Portales Valley probably formed on a low-density, porous H-chondrite asteroid by a high-energy impact event that caused crushing and melting; the target material was buried deeply enough to undergo slow cooling. Meteorites that appear to have formed, at least in part, by analogous processes include IIE-an Netschaëvo and EL6 Blithfield.

1. INTRODUCTION

The H, L, and LL ordinary chondrite (OC) groups constitute ~80% of all meteorites observed to fall (Graham et al., 1985). Individual OC are classified by thermal-metamorphic grade into four petrologic types (3, 4, 5, 6), reflecting increasing textural recrystallization, decreasing grain-to-grain variations in mineral compositions and decreasing bulk volatile element content (Van Schmus and Wood, 1967). Ninety-six percent of OC falls are classified into petrologic types 4–6 (Graham et al., 1985), indicating significant degrees of thermal metamorphism.

One of the major unsolved problems of planetary science is the identification of the mechanism or mechanisms responsible for heating chondritic asteroids. Those most often discussed are the decay of the short-lived radionuclide ^{26}Al ($t_{1/2}$ = 0.72 Ma) (Urey, 1955; Fish et al., 1960; Lee et al., 1976; Grimm and McSween, 1993), electromagnetic induction in the protosolar wind during an early T-Tauri phase (Sonett et al., 1970; Herbert et al., 1991), and collisional heating of large asteroids (Wasson et al., 1987; Cameron et al., 1990; Rubin, 1995a).

New petrologic evidence that impact phenomena can cause metamorphism and melting of chondritic material came in the form of the Portales Valley meteorite (Fig. 1a) which fell in Roosevelt County, New Mexico on 13 June 1998. A total of ~55 objects with a combined mass of ~106 kg was recovered (Kring et al., 1999; McHone et al., 1999). The three largest objects have masses of 34.0, 17.0, and 16.5 kg. Much of this report is based on a study of the latter specimen.

2. SAMPLES AND ANALYTICAL PROCEDURES

Sample numbers in the present paper are keyed to those in Table 1 of Kring et al. (1999). The 16.5 kg specimen is sample 1 on that list; clasts A, s1, s2, and s3 are from this specimen: the sample was cut into 14 pieces (Fig. 1b); clasts s1 and s2 are from slice 1j and are 9 cm apart; clast s3 is from slice 1e and is ~8 cm from clast s1. Clast D is from sample 3 (1600 g) on the Kring et al. (1999) list, clast E is from sample 16 (1472 g) and clast R is from sample 24 (128 g). Some observations were made on slabs cut by D. Pitt from sample 30 (6530 g). Clasts A, D, E, and R were studied as thin sections, clasts s1, s2, and s3 as thick slabs.

Four silicate clasts (A, D, E, R) were studied petrographically in thin section. Clast A is located adjacent to a 4 mm thick metal vein at the surface of the 16.5 kg specimen. Clast D is penetrated by a small metal vein. Clast E is located several centimeters from a metal vein. Clast R is from a small (128 g), metal-poor individual specimen of Portales Valley.

Metal and troilite grain sizes were measured in reflected light with a petrographic microscope. The longest dimension and the largest dimension perpendicular to it were averaged to determine the size of individual grains.

Mineral analyses were made with the Cameca electron microprobe at UCLA using natural and synthetic standards, 20 s counting times, and ZAF and PAP corrections. Modal analyses were made with the Zeiss universal petrographic microscope using an automated point counter. The density of the 16.5 kg specimen was determined by displacement using fine-grained rice and scales. A silicate-free metallic region was removed from a thick metal vein in a slice from a specimen belonging to M. Killgore. The metal was analyzed by instrumental neutron activation analysis (INAA) using previously described methods (Wasson et al., 1989).

In order to determine the metallographic cooling rate of the metal, we selected a field with a regular series of six taenite lamellae alter-

* Author to whom correspondence should be addressed (aerubin@ucla.edu).

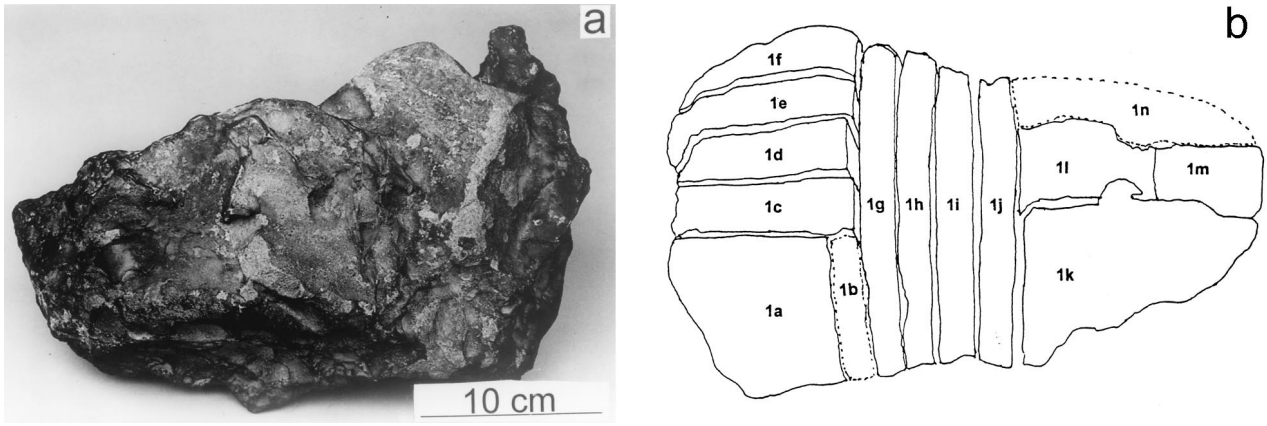

Fig. 1. The 16.5 kg specimen (sample 1) of Portales Valley containing coarse metal and silicate clasts of various sizes. (a) Photograph showing a large metal ridge forming a pinnacle above the rest of the specimen at right. Light-colored patches are silicate. (b) Schematic diagram of sample 1 after cutting, showing the relative locations of various slices. The sample is facing the opposite direction from the photograph in (a). Dashed lines indicate slices 1b and 1n which were retained by the Smithsonian Institution prior to the preparation of this diagram.

nating with kamacite bands. Profiles for Fe, Ni, and P were measured across each taenite lamella (typically 10–20 points) with the Cameca electron probe at 20 keV, 12 nA, and 20 s counting times. In most cases, the composition of the kamacite was determined by measuring four closely spaced points at the center of each kamacite band. In one case, we measured a complete profile from the center of the band to the adjacent taenite lamella with particular emphasis on the Ni-depleted zone near taenite. Due to the short counting time used, the precision for P was quite poor, but by pooling a total of 190 analyses we obtained an average P content of 0.01 wt.% in the bulk metallic Fe–Ni. After the microprobe work, the specimen was sectioned oblique to the taenite lamellae; the angle of the lamellae with the surface (53°) was used to correct the distance parameter in the profiles. Metallographic cooling rates were determined using the method of Rasmussen et al. (1995), taking into account variations in the local Ni content. We used profile-matching running simulations for the actual size of each cell and its integrated Ni content.

High-resolution x-ray computed tomography (HRXCT) of the 16.5 kg specimen of Portales Valley was done at the University of Texas at Austin (cf. Carlson and Denison, 1992). The three-dimensional data set consisted of 215 slices, each 2.0 mm thick, with an interslice spacing of 1.5 mm. With this resolution, metal ± FeS grains coarser than ~1.5 mm diameter are readily distinguishable from silicates. Imaging was done with a 420 kV tungsten x-ray source operating at 4.7 mA, prefiltered with 16 mm of brass. An integration time of 128 ms was used; 1600 views per slice were collected in 160% offset mode. The data set was digitally resectioned to permit examination of relationships in three mutually orthogonal orientations.

3. RESULTS

3.1. Petrography and Density

The most unusual textural feature of Portales Valley (Fig. 1a) is the high abundance and heterogeneous distribution of coarse metal. Some regions of the meteorite consist of large, angular silicate-rich areas (referred to here as clasts) embedded in metallic Fe–Ni (Fig. 2a); other regions consist of silicate-rich material traversed by narrow metal veins. The larger metallic patches range in size from 0.1 × 2 cm to 4 × 23 cm. In some cases, the silicates form multicentimeter-size angular clasts surrounded by metal (the largest silicate clast cropping out on the 16.5 kg specimen is 4 × 9 × 12 cm). In some clasts the interface between silicate and metal is straight, in others serrated or embayed. Heterogeneously distributed merrillite grains 50–150 μm × 200–300 μm in size occur at the boundary between silicate and the coarse metal. Ruzicka et al. (1999a) observed similarly situated merrillite and apatite grains up to 3 mm in size, and D. A. Kring and M. Killgore (personal communication, 1999) independently observed centimeter-size aggregates of phosphate grains near the coarse metal.

Some regions of the external surface of the 16.5 kg specimen contain prominent metal ridges that protrude up to 4 cm above the level of adjacent silicate clasts (Fig. 1); thinner metal veinlets typically 1–2 mm × 2–5 cm in size crop out between silicate clasts. In many cases, the veinlets delineate or cross 1–2 cm wide regmaglypts (thumb-print-shaped depressions formed at the surface of the specimen during atmospheric passage).

Although many shocked OC contain metal veins (e.g., Rubin, 1985; Stöffler et al., 1991), metallic regions as large as those in Portales Valley are not known in other OC. Metal-rich regions in Portales Valley typically contain abundant kamacite and minor taenite and plessite (Figs. 2b,c). The metal exhibits a prominent Widmanstätten pattern; kamacite has a mean bandwidth of ~0.5 mm, corresponding to Buchwald's (1975) division between fine and medium octahedrites. Ruzicka et al. (2000) reported rare centimer-size graphite nodules within the coarse metal.

Included within some patches of coarse metal are angular to rounded silicate clasts ranging in size from 0.5 mm to 7 cm (Fig. 2a). The HRXCT images show that most such isolated silicate clasts are the tips of larger clasts. Many clasts are angular; some have scalloped or irregular boundaries (Fig. 2d). Adjacent clasts separated by a metal vein commonly have complementary surfaces, implying only minor offsets following fracture. Many submillimeter-size silicate clasts occur in discrete clusters of 10 or so members surrounded by metal (Fig. 2a). Some of the images generated by HRXCT show metal containing small patches of numerous tiny silicate particles; these regions appear similar to the zones rich in small olivine particles in the Esquel pallasite (Ulff-Møller et al., 1998). Many small silicate particles are trapped at the side of larger silicate clasts. In large

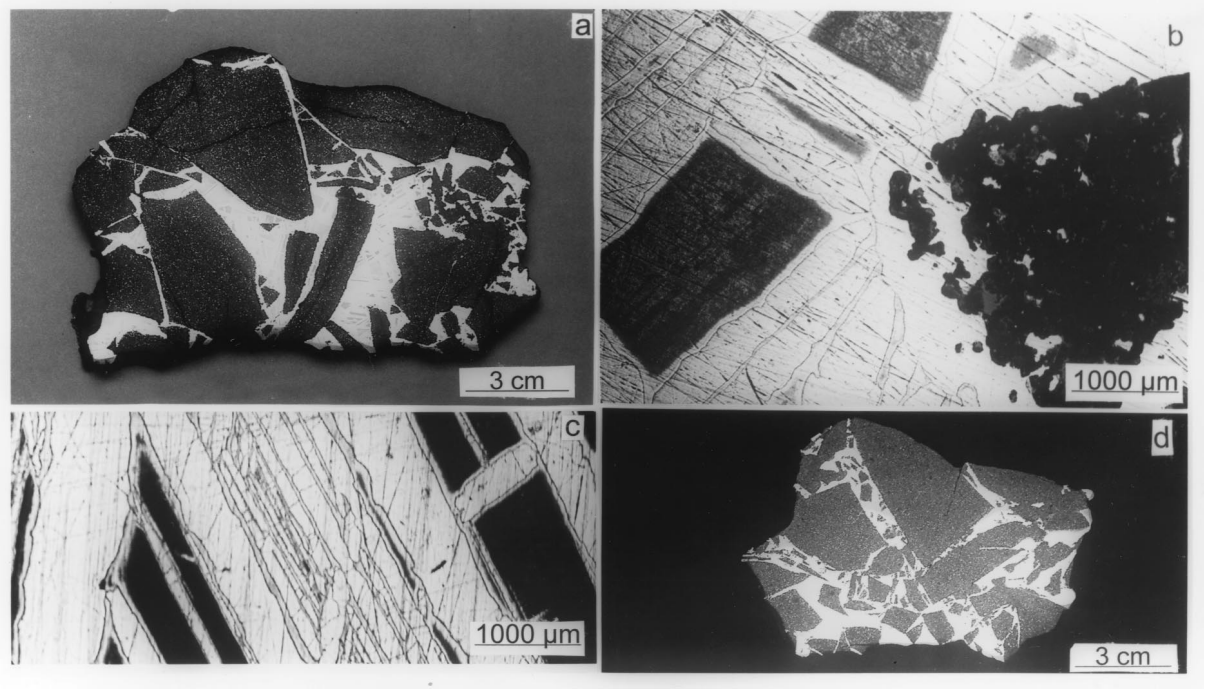

Fig. 2. Large-scale structure and Widmanstätten pattern. (a) Nital-etched slab of Portales Valley (cut from sample 3 listed in Table 1 of Kring et al., 1999) showing massive metal and narrow veins cross-cutting silicate clasts (dark gray) of different morphologies. Fine-grained silicate clast debris occurs at right. Clasts at left and at top appear to be a fractured block with metal filling the cracks. There are two distinct orientations of the Widmanstätten structure; the dividing line is the large elongated, quasirectangular silicate clast extending NNE from bottom center to just past the center of the slab. A thin sulfide vein (bottom right) extends from the edge of the metal into and across a large silicate clast. The uniformly distributed white dots in the silicate clasts are metallic Fe–Ni and troilite. (b) Detail of the Widmanstätten structure showing kamacite (white) swathing a silicate mass (dark gray at right). Approximately rectangular and triangular patches of plessite (medium gray) occur at left. (c) Typical Widmanstätten structure showing kamacite (white) intercalated with taenite (light gray); fine lines are polishing scratches. Triangular and rectangular fine plessitic regions (black) also occur. (d) Slab of Portales Valley showing triangular silicate clasts (dark gray) apparently aligned in a SE–NW direction within metal (white) at extreme left. All images in reflected light.

metal patches, there is a tendency for these clusters of silicate particles to be concentrated at one end of the patch (Fig. 3).

In general, thick bands of swathing kamacite occur along the boundaries with the silicate clasts (Fig. 2b); small (<50 μm size) clasts within the metal are also typically surrounded by swathing kamacite.

Clasts A and R are extensively recrystallized, metal-poor, troilite-rich materials. They contain 9.1 and 3.1 vol.%, respectively, of 200–800 μm size angular to scalloped mafic silicate grains and 1.3 and 2.6 vol.%, respectively, of relict chondrule fragments with barred olivine, granular olivine–pyroxene and porphyritic olivine–pyroxene textures (Fig. 4a). The coarse silicate grains and chondrule fragments are surrounded by numerous 10–50 μm size rounded to idiomorphic grains of olivine, orthopyroxene, and plagioclase, many with 120° triple junctures.

Clast R contains 8.3 wt.% metallic Fe–Ni grains (kamacite, taenite, and tetrataenite) averaging 50 $\pm$ 40 μm in width, 15.5 wt.% troilite grains averaging 90 $\pm$ 60 μm, ~0.6 wt.% chromite, rare grains of chlorapatite and $\sim 5 \times 10^{-3}$ wt.% metallic Cu (Table 1).

Clast A contains 3.4 wt.% metallic Fe–Ni grains averaging 45 $\pm$ 35 μm, 19.5 wt.% troilite grains averaging 85 $\pm$ 65 μm, ~0.4 wt.% chromite and $\sim 5 \times 10^{-3}$ wt.% metallic Cu (Table 1). The 6–60 μm size metallic Cu grains are associated with ~1% of the metallic Fe–Ni grains; most of the metallic Cu grains occur at the interface between metallic Fe–Ni and troilite.

Immediately adjacent to the metal vein near clast A is a dark 450 $\times$ 600 μm size patch containing ~20 vol.% chromite, ~0.4 vol.% troilite and ~0.2 vol.% metallic Fe–Ni, all embedded in plagioclase (Fig. 5). Chromite in the patch occurs as tiny (0.5–4 μm size) subangular grains forming several linear arrays and as larger (10–60 μm) rounded, angular and anhedral grains, some of which are intergrown. Similar chromite- and plagioclase-rich patches occur elsewhere in Portales Valley (D. A. Kring, personal communication, 1999).

Penetrating clast D is a 3.5 mm wide vein consisting of ~60 vol.% silicate clasts (ranging in size from 20 μm to 2.4 mm) and ~40 vol.% troilite-free metallic Fe–Ni; 11.3 vol.% of the thin section containing clast D consists of coarse metal from this vein. The only grain of troilite within the metal-rich portion of this vein is a 120 $\times$ 200 μm size saddle-shaped patch connecting two silicate clasts. However, troilite occurs as moderately large grains (95 $\pm$ 75 μm) within the silicate clasts and as coarse grains (averaging 250 $\pm$ 150 μm and ranging up to 0.2 $\times$ 1.9 mm) within the silicates at the edge of the vein (Fig. 6a,b). Very few relict chondrules (0.2 vol.%) occur in the thin

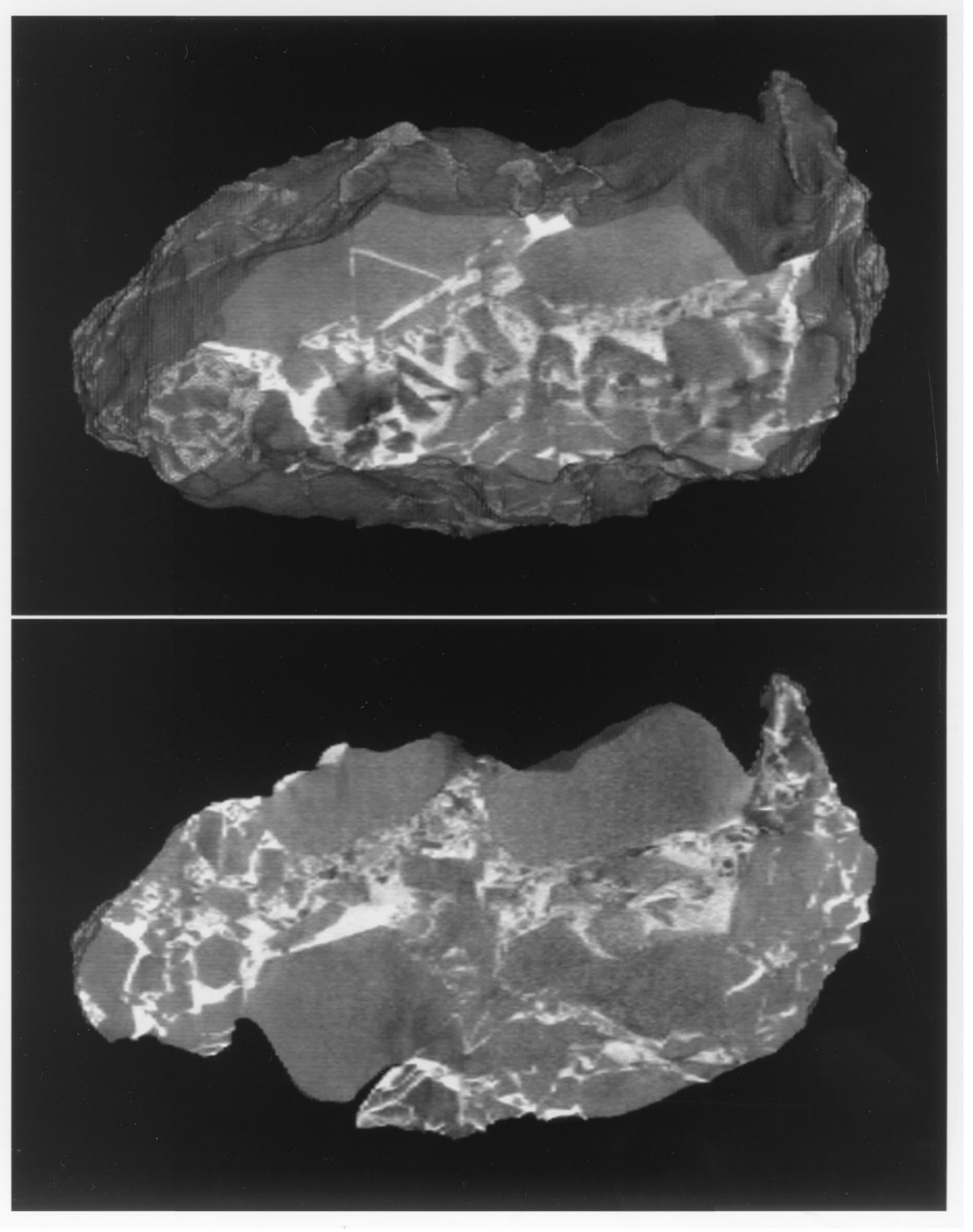

Fig. 3. High-resolution x-ray computed tomography (HRXCT) images showing the relationships between silicate clasts and metal veins in Portales Valley. Both images are "perspective views" that show what the meteorite might look like if a portion of it had been sawn or ground away to reveal an interior planar surface parallel to the page, with the remaining parts of the meteorite below the page. In the top image, the brightest whites (metal) lie in the page-parallel planar surface, and the surrounding material in darker shades is a rendering of the exterior surface below that level. In the lower image, deeper in the specimen, nearly all of the image is in the exposed planar surface. In both images, small silicate particles in the wider portions of the metallic regions tend to appear at the "top" of the veins; in the lower image, the bottom margin of the metallic region, particularly at left, has few particles in contact with it. These relationships suggest that where metallic regions were sufficiently large, silicate particles may have risen through the veins in response to gravitational forces, the direction of which would be vertical in these images.

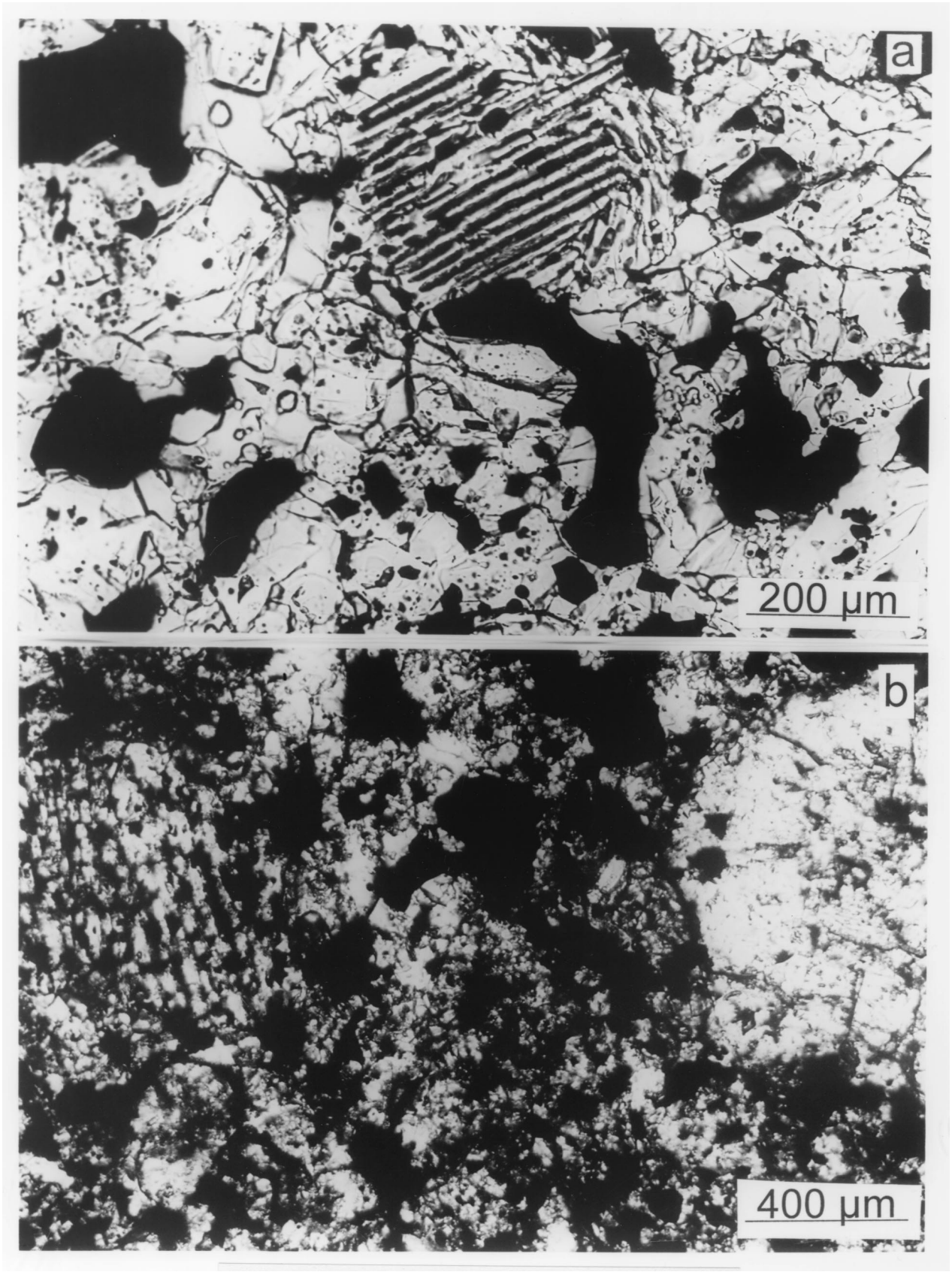

Fig. 4. Relict chondrules and silicate darkening in Portales Valley. (a) Clast A with a relict barred olivine (BO) chondrule surrounded by fine-grained silicates and troilite (black). The clast exhibits moderate silicate darkening due to the dispersion of small troilite blebs. (b) Extensive silicate darkening in clast E caused by tiny blebs of metallic Fe–Ni (black). Relict chondrules occur at both left and right. Both (a) and (b) in transmitted light.

Table 1. Modal abundances (wt.%; vol.% in italics) and grain sizes in Portales Valley clasts and H chondrites.

Mineral	Clast A	Clast D[a]	Clast E	Clast R	Clast s1	Clast s2	Clast s3	Mean H
Silicate	76.8 (*83.3*)	80.2 (*87.0*)	75.5 (*86.3*)	75.6 (83.5)	77.6 (*86.5*)	84.3 (*90.4*)	84.4 (*90.8*)	74.7
Fe–Ni metal	3.4 (*1.5*)	6.8 (*3.0*)	18.2 (*8.6*)	8.3 (*3.8*)	12.8 (*5.9*)	7.4 (*3.3*)	8.4 (*3.7*)	18.6
Troilite	19.5 (*14.9*)	12.5 (*9.6*)	5.5 (*4.4*)	15.5 (*12.1*)	9.3 (*7.4*)	7.9 (*6.0*)	7.1 (*5.4*)	5.3
Chromite	0.4 (*0.3*)	0.5 (*0.4*)	0.9 (*0.7*)	0.6 (*0.5*)	0.3 (*0.2*)	0.4 (*0.3*)	0.1 (*0.1*)	0.6
Metallic Cu	5×10^{-3} (2×10^{-3})	3×10^{-3} (1×10^{-3})	4×10^{-5} (2×10^{-5})	5×10^{-3} (2×10^{-3})				$\sim 10^{-4}$
Total	100.1	100.0	100.1	100.0	100.0	100.0	100.0	100.0
No. of points	1842	828	4540	6584	7488	5448	4840	
Area (mm^2)	40	85	260	387	2331	1504	560	

Weight percent was calculated from vol.% using the following mineral specific gravities: bulk silicate, 3.3; bulk metallic Fe–Ni, 7.95; troilite, 4.67; chromite, 4.7; metallic Cu, 8.95. H-chondrite normative mineralogy from Dodd (1981) also includes 0.6 wt.% apatite and 0.2 wt.% ilmenite. Metallic Cu data from Rubin (1994) have an uncertainty of about a factor of 2. Clasts A, D, E, and R studied in thin section; clasts s1, s2, and s3 studied in slabs cut from the 16.5 kg specimen.

[a] Modal abundances of minerals are normalized to 100 wt.% after exclusion of 22.0 wt.% coarse metal from an interpenetrating metal vein.

section containing clast D and the vein; ≥200 μm size mafic silicate grains are more common (8.1 vol.%). Clast D (including the vein) contains 27.3 wt.% metallic Fe–Ni. Most of the metal is in the vein which forms continuous metallic regions up to 1300 μm long; the remaining metal grains in the clast are 65 ± 40 μm across. The clast also contains 9.8 wt.% troilite, ~0.4 wt.% chromite and ~2×10^{-3} wt.% metallic Cu (Table 1).

Clast E consists of highly recrystallized chondritic material. It contains 18.2 wt.% metallic Fe–Ni grains averaging 120 ± 70 μm, 5.5 wt.% troilite grains averaging 75 ± 40 μm, ~0.9 wt.% chromite and ~4×10^{-5} wt.% metallic Cu (Table 1). Most of these values are very similar to those characteristic of H6 chondrites: 18.6 wt.% metallic Fe–Ni grains averaging 120 ± 150 μm, 5.3 wt.% troilite grains averaging 80 ± 60 μm, ~0.6 wt.% chromite and ~10^{-4} wt.% metallic Cu (Tables 1 and 2). Clast E contains 8.3 vol.% ≥200 μm size mafic silicate grains and 7.7 vol.% recognizable chondrule fragments; the corresponding values in typical H6 chondrites are 9.8 ± 2.1 and 11.4 ± 3.6 vol.% (Table 1). Olivine grains in the clast exhibit sharp optical extinction, characteristic of shock stage

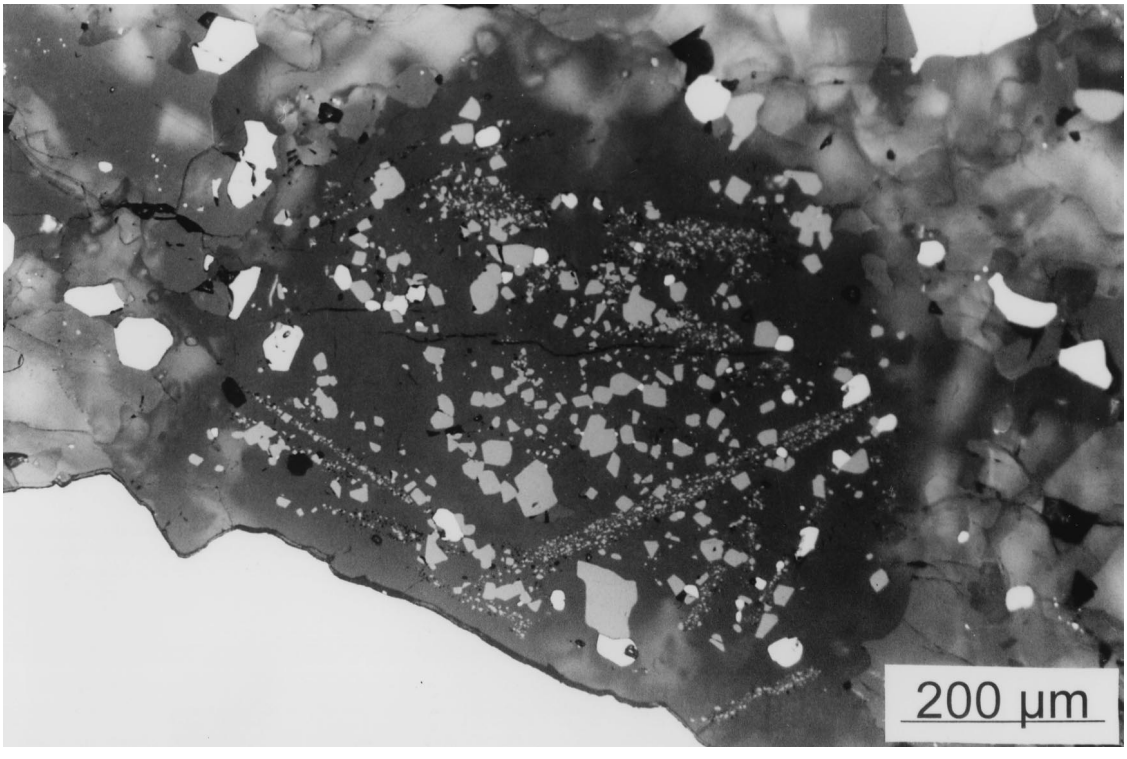

Fig. 5. Chromite-rich patch at edge of clast A. Chromite (light gray) occurs in small linear swaths oriented in two directions, relatively broad patches of small grains and as coarser, angular intergrown grains. The silicate material surrounding the chromite is crystalline plagioclase (dark gray). About two-thirds of the white grains touching some of the chromite grains are troilite; the remainder are metallic Fe–Ni. Coarse metal vein (white) is adjacent to the chromite-rich patch at lower left. Reflected light.

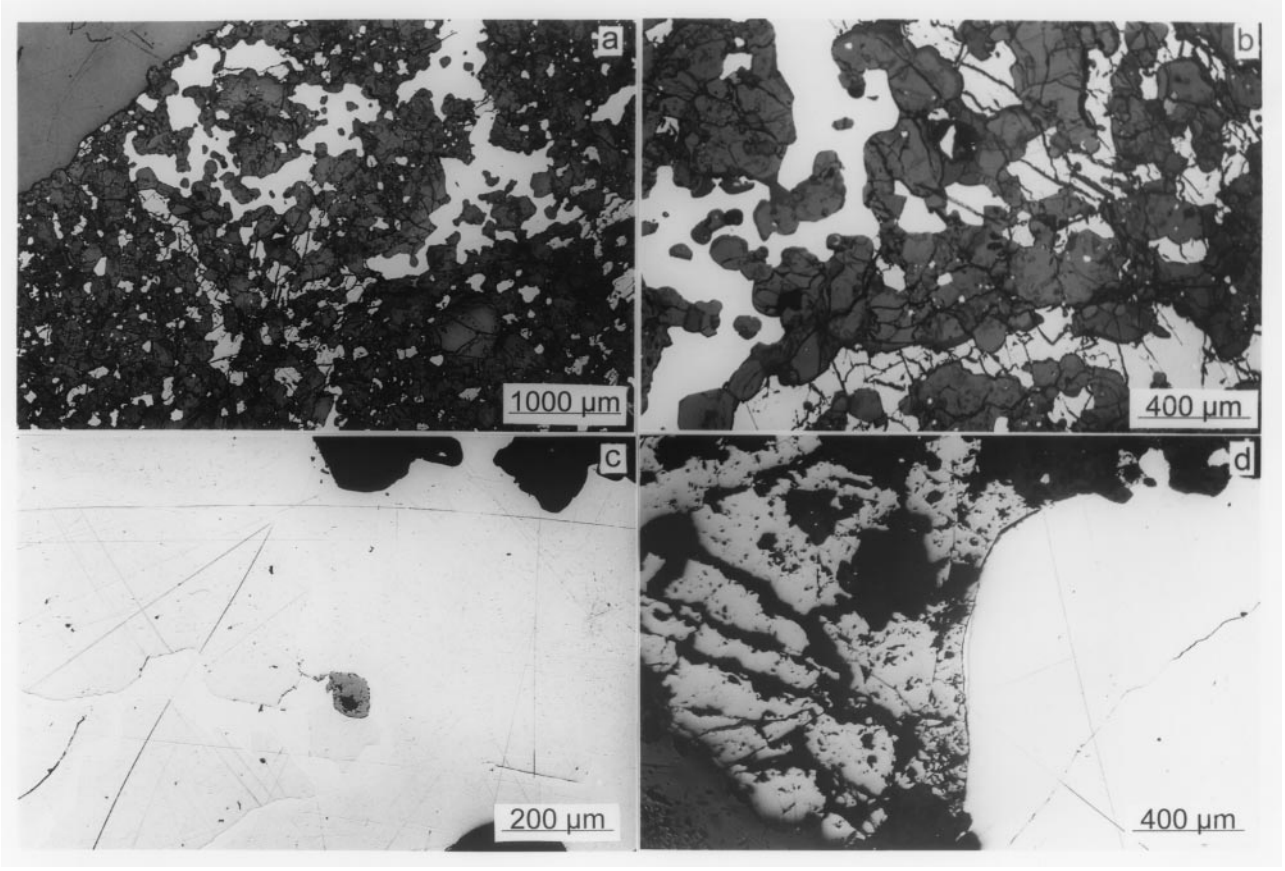

Fig. 6. Troilite and metallic Cu. (a) Portion of clast D near the edge of the metal vein (white) showing coarse, elongated grains of troilite (light gray) within silicate (dark gray). All of the metal in the image is part of a vein that contains a large proportion of silicate clasts. (b) Higher-magnification image of a portion of clast D shown in (a). Troilite forms elongated coarse grains and small rounded patches within silicate near edge of metal vein. (c) Small, rare, isolated troilite grain (medium gray) at the kamacite–taenite boundary within a coarse metal vein. (d) Massive patch of troilite (medium gray; left) at edge of coarse metal vein (white; right). A thin vein of metallic Cu (light gray) occurs at the interface between the metal and troilite. All images in reflected light.

S1, although a few grains with undulose extinction (S2) and planar fractures (S3) are also present. Many mafic silicate grains contain curvilinear trails of 0.2–25 μm size metal blebs; a few silicate grains contain thin (1 $\times$ 40 μm) troilite veinlets, chromite veinlets and rare curvilinear trails of 0.5–2 μm size chromite blebs. In transmitted light, these dispersed opaque grains cause extensive silicate darkening (Fig. 4b).

Modal abundances of silicates, metallic Fe–Ni, troilite and chromite were determined on three additional clasts from thick slabs cut from the 16.5 kg specimen (Table 1). The abundances

Table 2. Modal abundances (vol.%) and sizes of chondrules and particles in Portales Valley clasts and H chondrites.

Component	Clast A	Clast D	Clast E	Clast R	H5 (n = 6)	H6 (n = 5)	H3 (n = 1)
Relict chondrules	*1.3*	*0.7*	*7.7*	*2.6*	*22.1 ± 6.7*	*11.4 ± 3.6*	
No. of points	1436	1750	4744	3056	7485	5517	
≥200 μm silicates	*9.1*	*8.1*	*8.3*	*3.1*	*9.0 ± 2.1*	*9.8 ± 2.1*	
No. of points	1252	887	2396	1973	7914	6333	
Mean particle size (μm)							
Fe–Ni metal	45 ± 35	60 ± 40[a]	120 ± 70	50 ± 40	120 ± 150	120 ± 150	~65
No. of grains	50	40	50	50	150	175	78
Troilite	85 ± 65	95 ± 75[a]	75 ± 40	90 ± 60	75 ± 70	80 ± 60	30 ± 45
No. of grains	50	40	50	101	200	200	126

H5 chondrites include Anlong, Changde, Changxing, Enshi, Jilin, Mianchi. H6 chondrites include Butsura, Lunan, Wuan, Xingyang, Zhovtnevyi. The H3 chondrite data are from Sharps (Benoit et al., 1998).

[a] Grain sizes in clast D measured outside the coarse metal veins.

Table 3. Mean compositions and standard deviations (wt.%) of silicates and chromite in Portales Valley clast R.

No. of grains	Olivine 17	Orthopyroxene 17	Ca pyroxene 2	Plagioclase 20	Chromite 11
SiO_2	39.9 ± 0.3	57.0 ± 0.3	54.6 ± 0.3	66.6 ± 0.4	<0.04
TiO_2	<0.04	0.20 ± 0.03	0.58 ± 0.02		2.1 ± 0.3
Al_2O_3	<0.04	0.19 ± 0.02	0.61 ± 0.10	22.3 ± 0.2	7.0 ± 0.3
Cr_2O_3	<0.04	0.17 ± 0.04	1.0 ± 0.1		55.6 ± 0.6
FeO	17.4 ± 0.3	11.0 ± 0.2	4.2 ± 0.3	0.52 ± 0.11	27.9 ± 1.2
MnO	0.46 ± 0.04	0.49 ± 0.04	0.28 ± 0.06		0.77 ± 0.06
MgO	43.3 ± 0.3	31.2 ± 0.2	17.2 ± 0.2		3.7 ± 1.0
CaO	<0.04	0.79 ± 0.14	21.3 ± 0.7	2.8 ± 0.1	<0.04
Na_2O	<0.04	<0.04	0.56 ± 0.01	9.3 ± 0.3	<0.04
K_2O	<0.04	<0.04	<0.04	1.0 ± 0.2	<0.04
Total	101.1	101.0	100.3	101.5	97.1
Endmember	Fa18.4 ± 0.3	Fs16.3 ± 0.3 Wo1.5 ± 0.3	Fs6.8 ± 0.6 Wo43.9 ± 0.7	Ab80.8 ± 1.3 Or5.7 ± 1.2	

are 12.8 wt.% metal and 9.3 wt.% troilite in clast s1, 7.4 wt.% metal and 7.9 wt.% troilite in clast s2, and 8.4 wt.% metal and 7.1 wt.% troilite in clast s3. These clasts are all poorer in metal and richer in troilite than normal H chondrites (Table 1).

Although troilite is heterogeneously distributed in the massive metal, integration of large areas shows that the troilite/metal ratio in the metal is appreciably lower than the H-chondrite weight ratio of 0.28 (Table 1). Three distinct petrographic occurrences of troilite are associated with the coarse metal in Portales Valley: (1) Very rare <100 μm size isolated troilite grains occur within the metal patches (Fig. 6c). (2) Massive patches of troilite (≤1.2 mm in maximum dimension) are present in some areas at the boundary between the metal and silicate clasts. In some cases, metallic Cu rinds up to 420 μm long occur at the interface between the metal and troilite (Fig. 6d). A related occurrence of troilite consists of coarse grains within silicate near and at the boundary with the coarse metal. (3) Troilite also occurs in curvilinear veins up to 0.3×3 cm in size that extend from the metal–silicate boundary into the silicate clasts; in some cases there are small metal patches within the troilite veins.

We determined the density of the 16.5 kg specimen by displacement using fine-grained rice and a flat-bed scale. We obtained a result of 4.2 ± 0.1 g cm^{-3} (making the assumption of 0% porosity); this implies that the specimen contains ~35 wt.% metallic Fe–Ni, appreciably more than in typical H chondrites (18–19 wt.%; Table 1). In fact, some porosity is present as visible cracks in some metal–silicate boundaries; if we assume 5% porosity, the density increases to 4.3 g cm^{-3} and the metal fraction to 38%. An independent measure of the total amount of metal in this specimen is the quantitative analysis of the HRXCT images. These indicate that the coarse metal constitutes 22 vol.%, corresponding to 40 wt.% (assuming a density of 7.95 g cm^{-3} for the coarse metal and an average of 3.3 g cm^{-3} for the silicates). Unfortunately, these HRXCT images do not distinguish troilite from metal. Nevertheless, because of the generally low troilite abundance, the HRXCT value of 40 wt.% metal is probably more accurate than the density-derived value of 35–38 wt.%.

3.2. Mineralogical and Geochemical Properties

The silicate phases in the clasts include olivine, orthopyroxene (bronzite), Ca pyroxene (endiopside), and plagioclase (oligoclase). Also present in the silicate clasts are chromite, chlorapatite, merrillite, troilite, metallic Cu and the metallic–Fe–Ni minerals kamacite, taenite (containing 30.5–41.0 wt.% Ni) and tetrataenite (the single analyzed grain contains 50.0 wt.% Ni). Mineral compositions are summarized below and listed in Tables 3 and 4.

Olivine is homogeneous and has a mean Fa content (18.4 ± 0.3 mol.%; $n = 17$) characteristic of H4-6 chondrites (Fa 17.3–20.2; Rubin, 1990). The only minor element (expressed as an oxide) above the detection limit is MnO (0.46 ± 0.04 wt.%), which is also in the range of equilibrated H chondrites (Table A3.34 of Brearley and Jones, 1998).

Orthopyroxene is homogeneous and has a mean composition (Fs16.3 ± 0.3 Wo1.5 ± 0.3; $n = 26$) in the equilibrated H-chondrite range (Fs15.7–18.1 Wo0.9–1.5; Gomes and Keil, 1980). Minor elements (0.19 wt.% Al_2O_3, 0.49 wt.% MnO, 0.17 wt.% Cr_2O_3, 0.79 wt.% CaO and 0.20 wt.% TiO_2) are also within the established ranges of equilibrated H chondrites (Table 20 of Gomes and Keil, 1980).

Ca pyroxene is relatively rare; only two grains were analyzed. Their average endmember composition (Fs6.8 Wo43.9) is within the equilibrated H-chondrite range (Table A3.36 of Brearley and Jones, 1998). The minor elements are all within or near the H-chondrite Ca pyroxene ranges except for Cr_2O_3 (1.0 ± 0.1 wt.%) which is somewhat higher than those of

Table 4. Mean compositions and standard deviations (wt.%) of metallic Fe–Ni and troilite in Portales Valley clast R.

No. of grains	Kamacite 13	Taenite 6	Tetrataenite 1	Troilite[a] 6
Fe	93.8 ± 0.8	64.4 ± 4.9	49.6	63.4 ± 0.6
Co	0.55 ± 0.09	0.12 ± 0.06	<0.04	<0.04
Ni	6.4 ± 0.2	36.0 ± 4.7	50.0	<0.04
S				36.1 ± 0.3
Total	100.8	100.5	99.6	99.5

[a] Cr is below the detection limit of 0.04 wt.%.

Table 5. Comparison of Portales Valley clast R mineral compositions to those of H-group chondrites.

Mineral	Clast R	H range	Ref.
Olivine Fa (mol.%)	18.4	17.3–20.2	1
Low-Ca pyx Fs (mol.%)	16.3	15.7–18.1	2
Plagioclase Ab (mol.%)	80.8	79.2–82.9	3
Or	5.8	5.0–7.7	
Chromite TiO_2 (wt.%)	2.1	1.0–3.0	4
Cr_2O_3	55.6	31–58	
FeO	27.9	27–32	
MnO	0.77	0.6–1.4	
MgO	3.7	2–4.3	
Al_2O_3	7.0	4.2–7.3	
Kamacite Co (wt.%)	0.55	0.44–0.51	1

References: 1 = Rubin (1990); 2 = Gomes and Keil (1980); 3 = Van Schmus and Ribbe (1968); 4 = Brearley and Jones (1998).

typical H chondrites (0.4–0.7 wt.%; Table A3.36 of Brearley and Jones, 1998).

The plagioclase endmember composition (Ab80.8 ± 1.3 Or5.8 ± 1.2) is near the mean equilibrated H-chondrite plagioclase composition (Ab81.9Or5.8; Van Schmus and Ribbe, 1968); L and LL chondrites have slightly higher Ab and lower Or compositions.

Chromite in Portales Valley contains significant amounts of Al_2O_3 (7.0 ± 0.3 wt.%), MgO (3.7 ± 1.0 wt.%), TiO_2 (2.1 ± 0.3 wt.%), and MnO (0.77 ± 0.06 wt.%). It is closest in composition to chromite in equilibrated H chondrites (Table 5); although the MgO content is high, it is within the mode of Fig. 191b of Brearley and Jones (1998). The Al_2O_3 content of chromite in Portales Valley (7.0 ± 0.3 wt.%) is higher than that in any other equilibrated H chondrite (5.6–6.6 wt.%) except the Weston regolith breccia (7.3 wt.% Al_2O_3).

Troilite is stoichiometric FeS with Ni, Co, and Cr values below the detection limit of ~0.04 wt.%.

Three metallic–Fe–Ni phases are present in Portales Valley silicate clasts: kamacite with 6.4 ± 0.2 wt.% Ni and 0.55 ± 0.10 wt.% Co ($n = 9$), taenite averaging 36.1 ± 4.2 wt.% Ni and 0.11 ± 0.06 wt.% Co ($n = 6$) and tetrataenite with 50.0 wt.% Ni and <0.04 wt.% Co ($n = 1$). The analyses of the zoned grains reported here are the average compositions of the centers, edges, and regions half-way in between. The kamacite Co content is just above the normal H chondrite range (0.44–0.51 wt.%; Rubin, 1990), but is significantly lower than that of L chondrites (0.70–0.95 wt.%). In many kamacite grains, the Co content increases from grain centers toward grain edges (e.g., 0.54 vs. 0.58 wt.% in one grain) as expected during cooling (Afiattalab and Wasson, 1980). The kamacite Ni content is within the H-chondrite range (6.3–7.5 wt.%; Rubin, 1990). Kamacite grains are depleted in Ni at their edges by 16% relative to their centers (i.e., 5.4 vs. 6.4 wt.%). Taenite grains have M-shaped Ni profiles; in many cases, a rind of tetrataenite occurs at the taenite–kamacite boundary.

Similar zoning profiles occur in the metal lamellae that constitute the Widmanstätten pattern in the coarse metal: taenite has M-shaped Ni profiles, kamacite grains are depleted in Ni at their boundaries with taenite, and tetrataenite occurs along some kamacite–taenite boundaries. Samples etched with nital reveal numerous regions of comb plessite (cf. Buchwald, 1975), typically several millimeters in size, of roughly triangular and rectangular outline (Fig. 2b,c). Each plessite region is completely rimmed by a band of taenite that is scalloped in outline and tends to bend in toward the plessite and away from the surrounding kamacite.

Table 6. Composition of massive metal in Portales Valley and bulk metal in H chondrites.

	Sample 1	Sample 2	Mean metal	Mean H metal
Mass (mg)	607.4	641.6		
Cr (μg/g)	436	56	246	
Co (mg/g)	5.27	4.93	5.10	4.47[a]
Ni (mg/g)	88.9	105.1	97.0	87.6[a]
Cu (μg/g)	309	428	368	374[b]
Ga (μg/g)	16.7	19.1	17.9	14.4[e]
As (μg/g)	13.9	13.8	13.8	11.4[a]
Sb (ng/g)	297	409	353	360[a]
W (μg/g)	0.94	1.11	1.02	0.92[c]
Re (ng/g)	365	403	384	440[d]
Ir (μg/g)	3.27	3.49	3.38	3.12[c]
Pt (μg/g)	7.7	7.4	7.6	10.3[d]
Au (μg/g)	1.349	1.506	1.428	1.17[a]

[a] Whole-rock H chondrite ranges normalized from Kallemeyn et al. (1989) assuming that these elements are completely siderophile and that mean H chondrites contain 186 mg/g metallic Fe–Ni.

Mean H-chondrite metal data: [b] Rambaldi and Cendales (1979); [c] Widom et al. (1986); [d] Rambaldi (1977); [e] mean H4–H6 chondrite metal from Chou et al. (1973).

The Ni-normalized abundance ratios of elements in the bulk metal (as determined by INAA in a sample from an unnumbered coarse, silicate-free patch of metallic Fe–Ni) are similar to (generally within 20% of) mean metal in H4-6 chondrites (Table 6); however, the composition is somewhat fractionated. The most deviant elements are Pt and Re (depleted) and Co, Ga, As, and Au (enriched) relative to H chondrites. These trends are similar to those in the IIIAB magmatic iron meteorite group (e.g., Wasson and Richardson, 2001).

3.3. Shock Effects

Most coarse olivine grains in Portales Valley exhibit sharp optical extinction in the microscope, indicative of shock stage S1 (unshocked) (Stöffler et al., 1991). Nevertheless, a few grains exhibit undulose extinction (S2) and a few others contain planar fractures characteristic of shock stage S3, corresponding to a shock pressure of 5–10 GPa (Stöffler et al., 1991).

Some coarse olivine and orthopyroxene grains in relict chondrule fragments contain 20–300 μm long curvilinear trails of 0.4–6 μm size kamacite blebs (Fig. 7a). Such trails are similar to those responsible for the phenomenon of silicate darkening in highly shocked OC (Rubin, 1992) except that those in Portales Valley contain almost no troilite blebs and those in most shocked OC (e.g., Rose City; Rubin, 1992) are composed mainly of troilite. Clast E exhibits extensive silicate darkening (Fig. 4b).

A few mafic silicate grains in Portales Valley contain curvilinear trails of chromite blebs and small chromite veinlets 1–2 μm × 20–260 μm in size (Fig. 7b). Similar chromite veinlets have been reported previously in shocked OC (e.g., L6 Stratford, S4; LL4 Bo Xian, S3) (Rubin, 1992) and occur in OC impact-melt breccias (Rose City, S6; A.E. Rubin, unpublished observations). Although chromite veinlets also occur in some

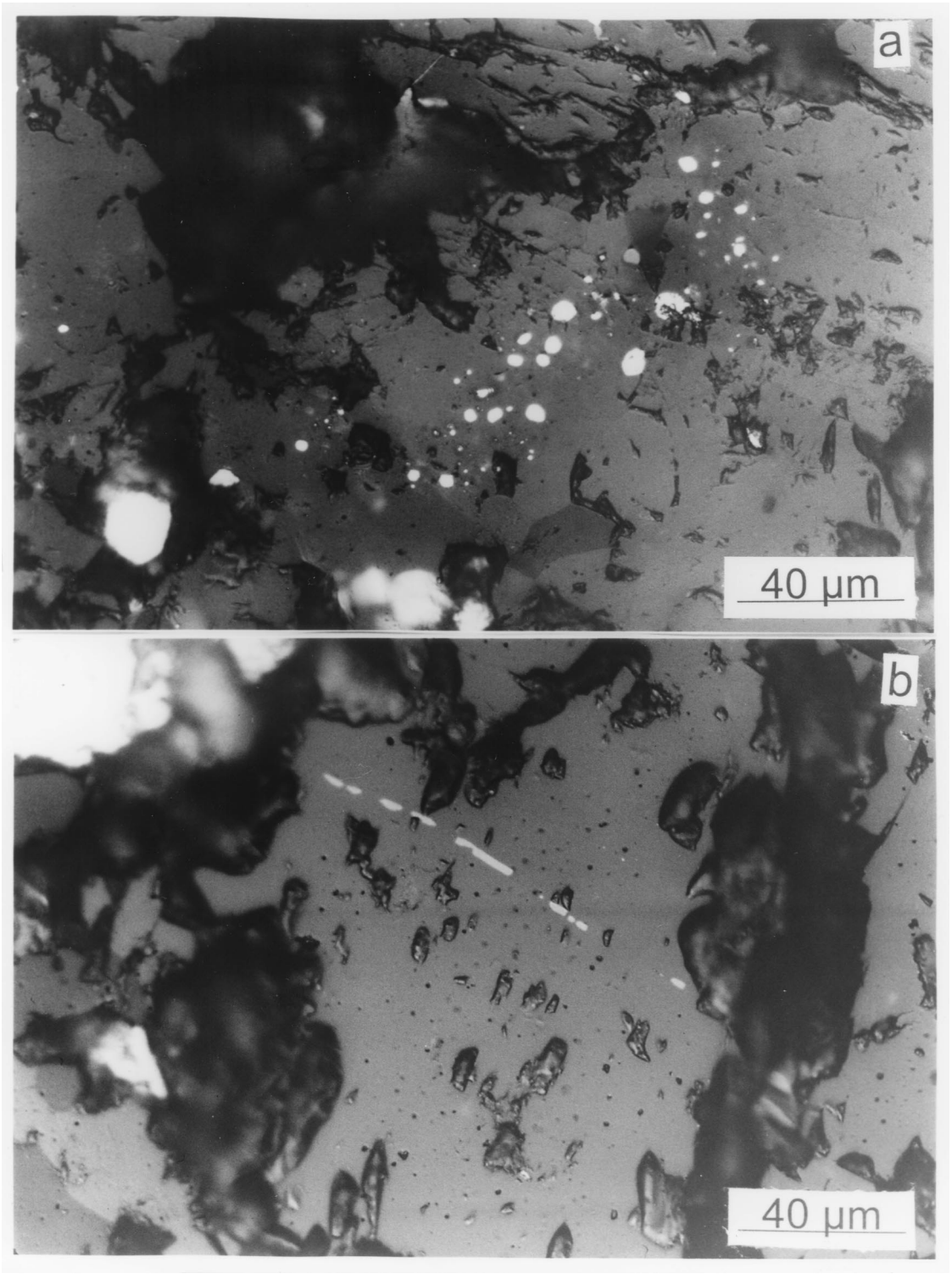

Fig. 7. Probable relict shock features. (a) Curvilinear trails of metallic Fe–Ni blebs (white) in relict mafic silicate grains (gray) in clast R. (b) Discontinuous chromite veinlet (light gray) within mafic silicate grain (medium gray) in clast R.

low-shock-stage S1 and S2 OC, the veinlets appear to be healed fractures, suggesting that the rocks may have been shocked and annealed. Kring et al. (1999) reported a 4 mm long vein of merrillite in Portales Valley that they attributed to shock metamorphism.

Another indicator of shock in Portales Valley silicates is the relatively high number of occurrences of metallic Cu (Fig. 6d) present mainly as irregular flecks and veins at metal–troilite boundaries. Clast A contains a 14 μm wide euhedral metallic Cu grain at the interface of troilite and

silicate. Rubin (1994) defined "occurrence abundance" (or "OA") as:

$$100 \times [(\text{number of occurrences})/\text{mm}^2].$$

Strongly shocked OC tend to have metallic Cu OA values ≥2.5; unshocked (S1) OC have a mean OA value of ~1. In Portales Valley silicates, the total number of occurrences of metallic Cu observed in thin sections of clasts A, D, E, and R is 24; the surface area of the thin sections is 549 mm^2, resulting in an overall OA value of 4.4. However, the highly recrystallized chondritic clast E has a low OA (0.8), while those of clasts A, D, and R are 20, 8.2, and 4.3, respectively, based on a surface area of 289 mm^2. The only comparable OA values among the 88 OC examined by Rubin (1994) for which thin sections having surface areas > 50 mm^2 were available are from Farmville (H4, S3, OA = 9.0) and Fukutomi (L5, S3, OA = 9.7). However, these values may not be representative because they are based on thin sections with only 67 and 62 mm^2, respectively, not far above the arbitrary 50 mm^2 cutoff. Thus, some regions of Portales Valley have the highest known occurrence abundances of metallic Cu among well-sampled OC.

4. DISCUSSION

4.1. Classification

Most classificatory parameters indicate that Portales Valley is an H-group chondrite (Table 5). The mean olivine, orthopyroxene and plagioclase compositions in clast R are within the established ranges for H chondrites (Table 5). Chromite is slightly poorer in Cr_2O_3 and FeO and somewhat richer in MgO and Al_2O_3 than that in mean equilibrated H chondrites, but each value is within the established H-chondrite ranges. The fine-grained kamacite within the Portales Valley silicate clasts contains 0.55 ± 0.09 wt.% Co, slightly outside the range of H chondrites (0.44–0.51 wt.%; Rubin, 1990), but far below the L-chondrite range (0.70–0.95 wt.% Co). Ruzicka et al. (1999a) reported that the REE abundances in merrillite and chlorapatite in Portales Valley are similar to those in metamorphosed OC; they further reported that the REE abundances in merrillite and orthopyroxene are similar to those predicted for an equilibrated H chondrite. The whole-rock O-isotopic composition of Portales Valley ($\delta^{18}O$ = +3.9‰; $\delta^{17}O$ = +2.7‰; $\Delta 17O$ = +0.67‰; R. N. Clayton, personal communication, 1998) is also characteristic of equilibrated H-group chondrites: $\delta^{18}O$ = +3.6–4.5‰; $\delta^{17}O$ = +2.4–3.2‰; $\Delta 17O$ = +0.53–0.86‰ (Clayton et al., 1991).

Clast E has H-chondrite-like abundances of metallic Fe–Ni and troilite (Table 1), although our section is slightly enriched in chromite and depleted in metallic Cu relative to mean H chondrites (Keil, 1962; Rubin, 1994). The sizes of the metal and troilite grains in clast E are about the same as those in H chondrites (Table 2; Figs. 8a,b) and the modal abundance of 8.3 vol.% ≥ 200 μm size mafic silicate grains is also in the H-chondrite range (Tables 1 and 2). It is clear that clast E is an H chondrite. The large degree of recrystallization of clast E indicates that it is petrologic type 6. The clast's abundance of recognizable chondrule fragments (7.7 vol.%) is at the lower extreme of those in typical H6 chondrites (11.4 ± 3.6 vol.%), indicating that an above-average proportion of chondrules in clast E may have been obliterated by intense recrystallization or a small degree of crushing or melting. (If the melting had exceeded ~10%, more chondrules would have been obliterated.)

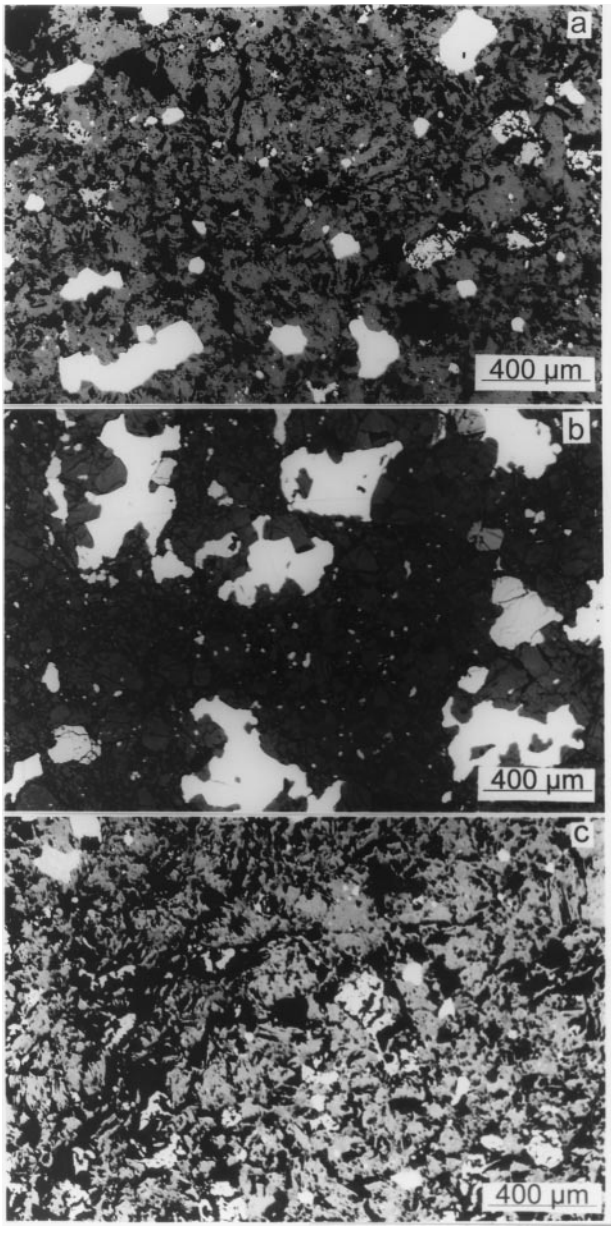

Fig. 8. Troilite and metallic Fe–Ni in Portales Valley and a normal H6 chondrite. (a) Clast E contains moderately coarse grains of metallic Fe–Ni (white) and troilite (light gray) surrounded by silicate (dark gray). There is a moderately high metal/troilite modal abundance ratio. The black areas are plucked regions. (b) The Lunan H6 chondrite fall contains coarse metallic Fe–Ni (white) and troilite (light gray) and has a similarly high metal/troilite ratio. (c) Clast R contains much more abundant troilite (light gray) and much less metallic Fe–Ni (white). The metal/troilite modal abundance ratio in this clast is far lower than in clast E or normal H6 chondrites such as Lunan; the troilite content of clast R is about three times higher than in Lunan. The black areas are plucked regions. All images in reflected light.

Clasts A and R (Fig. 8c) differ from normal H6 chondrites in

several important respects (Tables 1 and 2): (1) They are depleted in metallic Fe–Ni by factors of 5.5 and 2.2, respectively. (2) They are enriched in troilite by factors of 3.7 and 2.9, respectively. (3) They are depleted in ≥200 μm size mafic silicate grains by factors of 1.1 (not significant) and 3.2, respectively. (4) They are depleted in recognizable chondrule fragments by factors of 8.8 and 4.4, respectively. (5) They are enriched in metallic Cu by factors of 13 and 17, respectively.

If the coarse metal-rich vein is excluded from clast D, then this clast closely resembles clasts A and R in being richer in troilite than H chondrites (by a factor of 2.4), depleted in ≥200 μm size mafic silicate grains (relative to H6) by a factor of 1.2, depleted in recognizable chondrule fragments (relative to H6) by a factor of 16, and enriched in (recognizable) metallic Cu by approximately a factor of 10.

Relative to mean H chondrites, clasts s1, s2, and s3 are depleted in metallic Fe–Ni by factors of 1.4, 2.5, and 2.2, respectively, and enriched in troilite by factors of 1.8, 1.5, and 1.3, respectively.

The most significant departure from chondritic composition is in the troilite/metal ratios of clasts A, R, and D (5.7, 1.9, and 1.8, respectively); these values are 6.4–20 times greater than the corresponding ratio in mean H chondrites (0.28).

Although clast E can be classified as an H6 chondrite, the other clasts differ sufficiently in their modal mineral abundances, particularly in their troilite/metal ratios, that they cannot be classified as normal H chondrites. However, it seems most plausible that they were derived from normal H chondrite material; in the following section, we interpret the intermineral fractionations in clasts A, D, R, s1, s2, and s3 as being caused by impact melting of normal H chondrites.

4.2. Formation

There are several key properties of Portales Valley that must be explained by a successful model of its formation. These include (1) the characteristic structure of metal-rich regions, i.e., coarse metal with little associated FeS that fills the interstices among blocks of angular silicate clasts; (2) the presence of clasts having the texture and composition of normal H-chondrite materials; (3) the slow cooling necessary to grow large gamma crystals of metal and produce the fine-to-medium-grained lamellae of the Widmanstätten pattern; (4) the low abundance of chondrules and large mafic mineral fragments in many silicate clasts; (5) the low abundance of metal and high abundance of troilite in many silicate clasts; and (6) the high abundance of metallic Cu in many of the silicate clasts.

As discussed above, the presence of regions in Portales Valley that are "normal" H-chondrite material (e.g., clast E) makes it probable that such material was precursor to the materials that differ in composition and structure from normal H chondrites. One possibility is that the precursor material resembled clast E and was already recrystallized. Another endmember possibility is that the precursor was unmetamorphosed H3 material, possibly having a moderately high porosity.

Models that have been formulated to explain the key petrologic properties of Portales Valley include impact-melting of H-chondrite material (Rubin and Ulff-Møller, 1999) and internal heating of an H-chondrite asteroid, leading to extreme recrystallization and partial melting (e.g., Scott and Pinault, 1999).

4.2.1. Structural evidence that the metal-rich Portales Valley breccia was formed by an impact event

The Portales Valley structure is dominated by angular silicate clasts with metal filling the interstices between these clasts. We cannot find a plausible interpretation for producing this structure other than by crushing the silicates under circumstances in which the metal was molten. We can suggest two mechanisms that can cause crushing of silicates: (a) impact processes and (b) asteroidal tectonic forces unrelated to impact.

All asteroidal meteorites have experienced numerous impacts including those that compacted their porous nebular chondritic precursor materials into lower-porosity bodies, and those that liberated them from their parent body. In addition, genomict and polymict breccias experienced impact events that mixed clasts from different regions.

In contrast, there is no direct evidence for crushing associated with tectonic processes not produced by impacts. One possibility is that the main-group pallasites were produced by the collapse of an olivine mantle resulting from the contraction of a crystallizing metallic core, but if such a tectonic event occurred, it may equally well have been produced by an impact. There is no reason to suppose that the Portales Valley metal originated in a large (>10 m) metallic magma akin to those that produced magmatic irons and pallasites. We conclude that it is highly likely that the basic structure of the metal-rich Portales Valley samples was produced by an impact event.

4.2.2. Clast E: H-chondrite composition and structure and moderate shock effects

The fact that the least-altered samples of Portales Valley are more-or-less normal H chondrites is an important constraint on plausible models. As exemplified by clast E, Portales Valley is a normal H chondrite in terms of its silicate composition, chondrule abundances and textures, and metal and troilite abundances. In addition, the O-isotopic composition measured on another Portales Valley specimen is precisely that expected for an H chondrite. Therefore, it is probable that the metal-rich Portales Valley structure was produced by processes acting on normal H-chondrite materials.

Clast E records evidence of moderate shock effects. As reported above, some coarse mafic silicate grains and relict chondrule fragments contain curvilinear trails of tiny kamacite blebs (Figs. 4b and 8a) similar to those responsible for silicate darkening in OC of shock stages S3–S6 (e.g., Heymann, 1967; Smith and Goldstein, 1977; Rubin, 1992; Bennett and McSween, 1996). Also present in a few mafic silicate grains are curvilinear trails of chromite blebs and small chromite veinlets (Fig. 7b).

The characteristic H-chondrite-like modal abundances and grain sizes of metallic Fe–Ni and troilite in clast E indicate that this clast experienced little or no melting. Its modal abundance of recognizable chondrule fragments (7.7 vol.%) relative to those in normal H5 and H6 chondrites (22.1 ± 6.7 and 11.4 ± 3.6 vol.%, respectively; Table 1) can be accounted for by a slightly higher than average degree of recrystallization than in

typical of type-6 materials. A minor amount of melting may have occurred, but large (>1 mm) melt pockets or melt veins should still be recognizable after metamorphism, and these have not been found. We suggest that any melting of this clast involved <~10% of the silicates.

4.2.3. Evidence that the massive metal in Portales Valley was molten

There are two related problems involved in the production of the massive metal in metal-rich Portales Valley samples: (1) How was this metal separated from the parental H-chondrite silicates? (2) Was the metal ever fully molten? We know from studies of heavily shock-altered chondrites such as Rose City (Rubin, 1995b) that impact processes can produce metallic veins. There is also evidence that the large (centimeter-size) metal nodules in some unmelted H chondrites (e.g., Widom et al., 1986) are produced by impacts (e.g., Rubin, 1999). In some cases, these nodules are connected with veins inferred to have served as conduits for the formation of these nodules by the flow of molten metal into cavities produced by impact processes. It therefore seems to be only a minor extrapolation to conclude that the massive metal in Portales Valley was produced by impact-generated flow.

Because metal is ductile, it is possible to achieve a certain amount of flow by impact generated shear of high-viscosity metal at temperatures below the solidus. Such a process, however, would entrain silicate fragments, as observed in Rose City; it cannot explain the fact that many of the massive metal regions in Portales Valley are largely free of silicates. In some regions having areas >7 cm^2 we could not find any silicate fragments at all. If we assume that the precursor of Portales Valley was a normal H chondrite, it follows that the coarse metal consisted initially of millimeter-size grains dispersed among silicates. We conclude that the only plausible way the metal could have become free of fine-grained silicates is by the buoyant separation of the silicates from molten metal having a relatively low viscosity. (We suggest that any micrometer-size silicates trapped in the metal subsequently dissolved as a result of their high surface energies, with their constituent atoms diffusing to larger silicate grains.)

Nevertheless, some thick metal-rich regions contain clusters of silicate particles concentrated at one end (Fig. 3). This texture may indicate that small silicate particles rose through large molten metal pockets in response to gravitational forces.

The inference that the coarse metal interstitial to the silicates was once molten is consistent with the HRXCT images that show complete interconnection of the regions of coarse metal throughout the three-dimensional volume of the specimen. We also confirmed the three-dimensional interconnectedness of coarse metal by using an ammeter to show that current flowed from widely separate metal outcrops on the exterior of the 16.5 kg specimen. Textural relationships are consistent with the metal having been molten when it invaded the (mostly) solid silicate: (1) Thin, continuous veins of metal penetrate deeply into some silicate clasts. (2) A few silicate clasts have scalloped and rounded margins at their interface with metal, consistent either with minor silicate melting or metamorphic recrystallization of some sharp angles. (3) Some small angular silicate fragments appear completely enclosed in metal, consistent with immersion in a metal melt.

4.2.4. More extensive shock effects in other silicate clasts

The nature of the impact products will depend on the scale of the impact event, the petrologic type of the precursor target material and on its texture, particularly its porosity. If all of the clasts in Portales Valley started out as H-chondrite material similar to the progenitor of clast E and if all of the clasts experienced the same degree of recrystallization as clast E, then the very low modal abundances of recognizable chondrule fragments in clasts A, D, and R (1.3, 0.7, and 2.6 vol.%, respectively) relative to that in clast E (7.7 vol.%) must be due to some chondrule-destroying process other than recrystallization. Such processes include pervasive crushing and melting (perhaps 20–40%).

Clast A contains a relict 300 μm diameter barred olivine chondrule (Fig. 4a) that is partially surrounded by 20–60 μm thick patches of olivine that appear to have grown epitaxially on the chondrule margins. Three thick parallel, adjacent olivine bars extend 60–70 μm beyond the apparent chondrule margin into the surrounding silicates. The olivine comprising the extension of these bars appears to have formed by nucleation and growth from a crystallizing melt. Some of the nearby troilite grains have partially rounded and scalloped morphologies, also consistent with moderate melting. Clast A also contains numerous 20–50 μm size droplet-shaped plagioclase patches, many in contact with scalloped-edge troilite grains. These textures suggest that some silicate melting has occurred in the clast. Melting is also suggested by the occurrence of curvilinear trails of metal blebs in the silicates.

4.2.5. Chromite

In shocked chondrites, some chromite occurs as small rounded to subangular grains dispersed in albitic glass; these have been reported in the Ramsdorf impact-melt breccia (Begemann and Wlotzka, 1969), the Smyer H-chondrite impact-melt breccia (Rubin and Arnold, 2000), L6 Kyushu (Ashworth, 1985) and in melt pockets of several other shocked L6 chondrites (Dodd and Jarosewich, 1982). Paranaiba (L6) contains chromite droplets dispersed within maskelynite (Keil et al., 1977). Another probably related inclusion is in L6 Los Martinez; it consists of crystalline plagioclase intergrown with chromium-rich spinel (Brearley et al., 1991). It seems plausible that all of these assemblages formed by shock melting; we speculate that a plagioclase–chromite association has a relatively low impedance to shock compression. Either the chromite in the mixtures happened to be adjacent to plagioclase prior to the shock event that melted it, or the chromite–plagioclase associations represent the impact-melt products of a primitive chromite-rich chondrule mesostasis. Such mesostases have been reported in chromite-bearing silicate chondrules (Ramdohr, 1967; Krot and Rubin, 1993).

A possible nebular scenario for producing the plagioclase–chromite association is the condensation of Na onto spinel substrates that may have had appreciable chromite contents. The resulting assemblage was probably poorly crystalline or even amorphous. During chondrule formation some occur-

rences of this assemblage would have been converted to a mixture of glassy mesostasis, possibly containing some fine chromite. Impact heating of this assemblage could produce a chromite–plagioclase melt.

In Portales Valley, the intergrown chromite grains and swaths of tiny aligned chromite crystals in the chromite- and plagioclase-rich patch adjacent to clast A (Fig. 5) were probably formed by impact mobilization. It is plausible that the chromite grains were initially surrounded by glass, but that subsequent annealing devitrified the glass and transformed it into crystalline plagioclase. The chromite grains may have been aligned by shock-induced shear or injection into a pre-existing fracture.

4.2.6. Metal and sulfide

The massive metallic regions were probably derived from the silicates by impact-induced (incomplete) melting of the silicate-rich clasts and formation of a metallic melt that separated from the crushed and partly melted silicates. Loss of metallic Fe–Ni could account for the low metal contents of clasts A, D, R, s1, s2, and s3 (3.4–12.8 wt.%) relative to mean H chondrites (18.6 wt.%), reflecting a loss of 30–80% of the metal initially present. (The clast D abundances exclude the coarse metal vein.) However, because troilite should have dissolved in the metallic liquid and thus been lost along with the metal, this process cannot account for the high troilite abundances in the clasts (7.1–19.5 wt.%) relative to mean H chondrites (5.3 wt.%). The FeS would have been incorporated into the melt more efficiently than metal, and thus should be even more depleted relative to mean H chondrites.

This suggests the possibility that clasts A, D, R, s1, s2, and s3 lost essentially all of their troilite and most of their metal during impact-induced incomplete melting and that most of the troilite was subsequently introduced. A possible mechanism for the introduction of metal and troilite is invasion of the silicates by a residual S-rich metallic melt. If this had occurred, the FeS should mainly form veins or stringers. There is petrographic evidence that this process occurred: thin troilite veins extend from the edge of the coarse metal far into some silicate clasts; coarse, elongated troilite stringers occur within the silicates at the edges of some metal veins (Figs. 6a,b) and some relatively large masses of troilite occur at the metal–silicate interface (Fig. 6d). In many cases, apparently isolated troilite grains (separated by distances up to ~1 cm) near the margin of metal veins are in optical continuity, indicating that they are part of a single troilite crystal (Pinault et al., 1999a) plausibly crystallized from a melt.

The original impact-induced expulsion of FeS and metal from the silicate clasts probably also involved some crushing and melting of the silicates. The filling of the interstitial regions with (largely) clast-free, low-FeS metal implies relatively high temperatures, ≥1750 K, the melting temperature of metallic Fe–Ni containing ~1% S (Brandes and Brook, 1998). At this temperature, there should have been an appreciable S_2-rich vapor associated with the metallic liquid. We suggest that condensation of the S_2 vapor was responsible for the reintroduction of much of the S into the silicates. The postulated vapor would have permeated the fractures in the crushed, partly melted silicate clasts, condensing on many of the remaining metal grains and transforming them into FeS. Some Fe may have also entered the silicates as a vapor. Troilite-rich regions in the Smyer H-chondrite impact-melt breccia appear to have formed in a similar manner (Rubin and Arnold, 2000).

4.2.7. Slow cooling

Differently oriented Widmanstätten patterns are discernable on the left and right sides of the large Portales Valley slab in Figure 2a; the large sizes (>6 cm) of these regions indicate that cooling was slow enough to allow multi-centimeter-size gamma grains to grow. Thus, the metal cooled through the γ field relatively slowly. If the liquid metal had instead quenched to low temperatures soon after formation in an impact event, it would have resembled the metal in the Rose City impact-melt breccia in consisting of rounded dendrites of martensite partially rimmed by scalloped masses of troilite (Fig. 9), both mixed with silicates.

In order to determine the metallographic cooling rate, we used profile-matching simulations for the size of each cell and its integrated Ni content (Rasmussen et al., 1995). It was impossible to match the calculated profiles with the data for any cooling rate. The character of the misfit reflects the way an increased P content affects the phase boundaries in the Fe–Ni system: higher P results in higher Ni in kamacite and lower Ni in taenite at the relevant temperatures. By trial and error we found that by using an initial content of 0.08 wt.% P, we can reproduce 11 of the 12 profile simulations with a cooling rate of ~10 K Ma^{-1} through 500°C. (Although the metallic Fe–Ni contains only 0.01 wt.% P, the occurrence of Ca-phosphate grains adjacent to the metal suggests that the P content of the metal was initially higher. We searched for, but failed to find, schreibersite grains in the coarse metal.)

We speculate that, after the precipitation of γ-iron, a substantial fraction of the P diffused out of the metal, was oxidized and formed Ca phosphate (e.g., Murrell and Burnett, 1983) at the metal–silicate interface (Ruzicka et al., 1999a).

The effects of slow cooling are recorded in additional assemblages: the Ni depletion at the edge of kamacite grains adjacent to taenite (both in massive metal and in metal within the silicate clasts; Ruzicka et al., 1999b; present study), the presence of tetrataenite among the metal grains in the silicate clasts, and the recrystallized texture of small silicate grains (many of which have triple junctures at angles close to 120°). This indicates a high degree of textural equilibrium, consistent with the original classification of Portales Valley as petrologic type 6.

During cooling, Portales Valley became highly recrystallized. As noted above, there is petrographic evidence in clast A for moderately extensive (20–40%) melting in the metal-depleted clasts. Materials that had remained solids served as nucleation substrates when these melts crystallized. In the surviving olivine grains, the previous shock-induced damage of the crystal lattice was healed, lowering the apparent shock stage of the rock to S1. This is consistent with the results of Bauer (1979) who observed healing of shock-induced microfractures in olivine grains from dunite charges that experienced shock pressures > 57 GPa.

Some shock features can survive annealing (Rubin, 1992). Those that occur in Portales Valley include curvilinear trails of opaque blebs in the silicates (i.e., the cause of silicate darkening), chromite veinlets in silicates and the presence of numer-

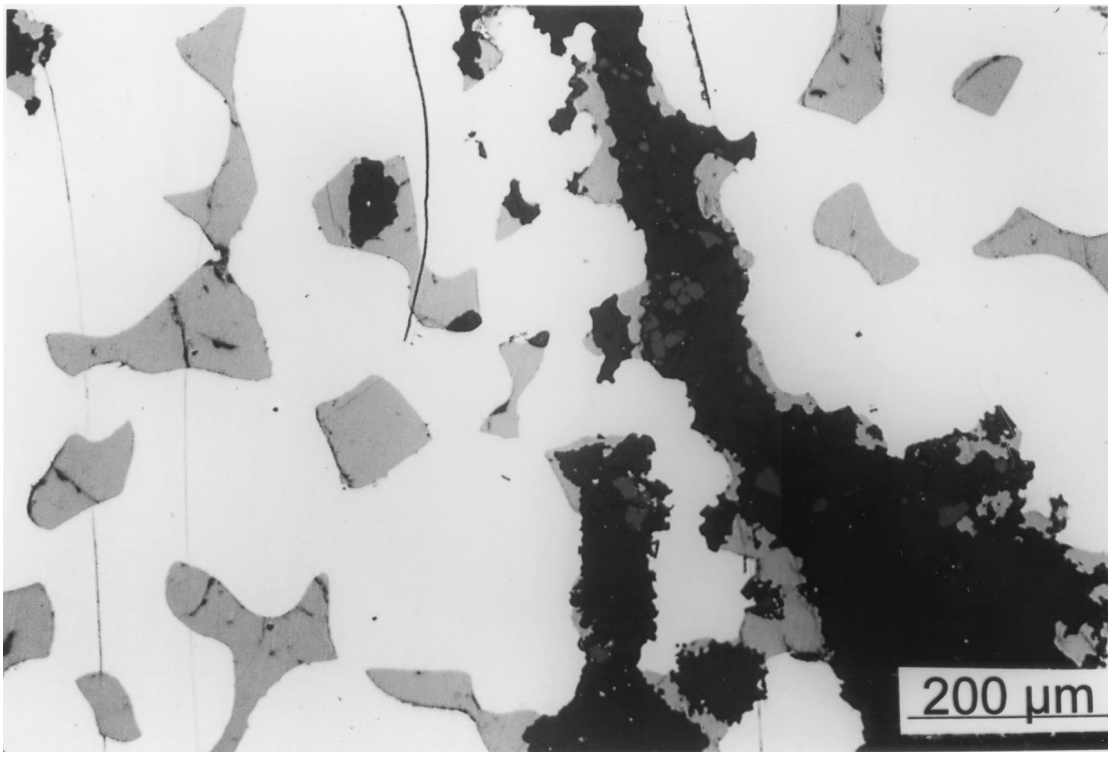

Fig. 9. Portion of a quenched S-rich metal vein in the Rose City H-chondrite impact-melt breccia showing metal dendrites (white) partially surrounded by scalloped troilite patches (light gray). Also present is a melted silicate inclusion (dark gray) containing chromite grains (medium gray). The silicate also served as a nucleation site for some troilite; small troilite patches occur along most of the metal–silicate boundary. This quenched metal–sulfide melt is far richer in troilite than the massive metal in Portales Valley; this indicates that the Portales Valley metal had a different thermal history that allowed loss of its initial allotment of troilite. Reflected light.

ous metallic Cu grains. Whereas the opaque grains forming curvilinear trails in shocked but unannealed rocks like Rose City consist of small blebs of metallic Fe–Ni and troilite, almost no troilite is present in the opaque trails within silicates in Portales Valley, the Netschaëvo IIE-an iron (this study) and in annealed chondrites such as H6 Kernouve (this study). It seems likely that during annealing of these meteorites, S was lost mainly from high-energy surface sites such as fractures, tiny crystals, and crystal edges (Lauretta et al., 1997). Because the tiny troilite blebs in the curvilinear trails have high surface-area/volume ratios, they are high-surface-energy sites and are likely to lose S to coarser sulfide grains. The small troilite blebs within the curvilinear trails of opaques in the silicates are thereby transformed into metallic Fe; additional annealing tends to bring an equilibrium amount of Ni into the metal blebs.

Although bulk-density determinations indicate that many samples of Portales Valley in our collections are enriched in metal (this study; Kring et al., 1999) (and, perhaps, also in troilite) relative to normal H chondrites, it is unlikely that these samples are representative of the entire parent body.

4.2.8. Cosmic-ray exposure age

The long cosmic-ray exposure (CRE) ages of most irons and stony irons relative to chondrites (e.g., Voshage, 1967; Crabb and Schultz, 1981) indicate that metal-rich meteoroids can survive the rigors of micrometeoroid impacts in interplanetary space for much longer periods than chondrites. For example, only ~5% of normal H chondrites have ages > 40 Ma (Graf and Marti, 1995), whereas >95% of iron meteorites have ages exceeding this value (Voshage, 1967). The relatively long (~40 Ma) CRE age of Portales Valley (D. D. Bogard, personal communication, 1999) could reflect an enhanced survivability of the metal-rich Portales Valley meteoroid.

4.3. The Heating and Melting of Portales Valley

We examined two endmember models for the formation of Portales Valley: impact-melting and internal heating. These differ in a fundamental respect: during impact heating, heat is deposited essentially instantaneously, but during internal heating, heat deposition typically occurs over periods exceeding one million years.

4.3.1. Comparison of impact-melting and internal heating models

During an impact event, each hypervelocity shock wave passes in less than a second, and successive hypervelocity waves (including reflected waves) can lead to appreciable heating resulting from highly localized stress concentrations (Rinehart, 1968). Immediately after the impact event materials separated by only several centimeters may have very different

temperatures, depending on the amount of shock-induced shear that they experienced during the impact.

In contrast, internal heating is a very slow process. The heat source, whether ^{26}Al or solar-wind induction, is more-or-less homogeneously distributed. At burial depths of several kilometers (i.e., several times the thermal diffusion length during one ^{26}Al half-life) there will be essentially no thermal gradients (these will develop after the decay of the ^{26}Al as a result of heat loss by radiation from the surface).

Another argument for a heterogeneous distribution of heat is that the metal-rich regions were completely molten whereas many silicate clasts were not. To calculate the temperature of the metal melt we assume that the melt included the rare FeS inside the coarse metal patches as well as the more common FeS situated at the boundaries between silicate clasts and massive metal. An approximate composition of this material is 88 wt.% Fe, 10 wt.% Ni, 1 wt.% S and 0.6 wt.% Co. According to the Fe–Ni–S phase diagram, the liquidus temperature of this mixture is $\approx$1750 K. However, at this temperature the silicates would be at least 40% melted; all the plagioclase would be in the melt as well as significant fractions of the pyroxene and olivine. Although some silicate clasts probably experienced such high degrees of melting, many silicate clasts retained their angular shapes, indicating that their initial melt fractions were much smaller. If the mean temperature of the silicates were 1600 K, then they would have experienced about 25–30% melting (Jurewicz et al., 1993).

Thus, immediately after the heating event, the massive metal melted completely, the adjacent silicate clasts experienced extensive melting, and materials like clast E located a few centimeters away, experienced $<$10% melting. We suggest that the mean post shock temperature of the metal was $\geq$1750 K; the mean temperature of the silicates was probably 100–300 K lower. Heat from the metal leaked into the adjacent silicates causing minor fractions to melt under static conditions that permitted them to retain their angular shapes. This is consistent with the fairly normal abundances of chondrules and coarse mafic grains in clast E and the anomalously low abundances of these constituents in clasts A, D, and R.

In many cases after impact melting and subsequent annealing of metal–sulfide assemblages, metallic Cu tends to nucleate and grow on metal–troilite interfaces. The high occurrence abundance of metallic Cu in many Portales Valley silicates is consistent with the impact-melting model and inconsistent with internal heating.

4.3.2. Collisional heating of porous asteroids

As discussed above, we conclude that Portales Valley was not heated by an internal source such as the decay of ^{26}Al or by solar-wind induction because there is strong evidence that the heat was deposited heterogeneously. In contrast, impact heating can provide a heterogeneous deposition of heat. The evidence of brecciation and other impact effects in the silicates (i.e., curvilinear trails of small metal blebs, chromite veinlets, and numerous occurrences of metallic Cu) are consistent with much of the metal and troilite having been melted by an impact. Some silicate regions (e.g., the progenitors of clasts A, D, and R) appear to have been appreciably melted. The slow cooling rate of the coarse metal probably reflects deep burial beneath low-thermal-diffusivity material such as regolithic debris. Kring et al. (1999) argued that such slow cooling rates might be expected beneath the floors of large ($\geq$20 km) impact craters on porous, rubble-pile asteroids. The impacts that produce rubble-pile asteroids offer a natural mechanism to achieve deep burial. Thick insulating layers of fine-grained crushed debris overlying the most strongly heated target rocks would cause this material to cool very slowly.

Various authors have questioned collisional-heating models in the literature. However, most of these criticisms do not apply to impacts into porous bodies (leading to a relatively efficient conversion of kinetic energy to heat) and to noncratering collisions that cause disruption followed by gravitational reassembly. Theoretical studies of the collisional evolution of asteroids (e.g., Davis et al., 1979; Hartmann, 1979) indicate that for a large range in impact energies, collisions can disrupt asteroids but fail to impart sufficient kinetic energy to most of the fragments to cause permanent dispersal. The disrupted material falls back together to form a rubble-pile asteroid that efficiently retains much of the heat generated in the collision.

There is increasing evidence that many asteroids are rubble piles with no effective tensile strength. In fact, asteroid 253 Mathilde appears to be a rubble pile of low density (1.3 ± 0.2 g cm^{-3}; Veverka et al., 1997; Yeomans et al., 1997) and high porosity ($\sim$50%; Cheng and Barnouin-Jha, 1999) although the size distribution of voids is not yet known. Harris (1996) identified an abrupt cutoff at the high end of the distribution of asteroidal rotation rates and concluded that most asteroids are rubble piles with no tensile strength. Bottke et al. (1999) examined the shape of near-Earth asteroids and concluded that some may have been molded by planetary tides; if so, they must be rubble piles with no effective tensile strength. This is consistent with radar images of some near-Earth asteroids in which these bodies appear to be aggregated boulders (e.g., Ostro et al., 1995).

During impacts kinetic energy is converted into heat largely by $P \cdot \Delta V$ effects, where P is the pressure and ΔV the change in volume. The greater the porosity, the larger is ΔV, and the more efficient is the conversion of kinetic energy to heat (Melosh, 1989; Housen and Holsapple, 1999). It is thus plausible that Portales Valley formed by a high-energy impact into a large, porous H-chondrite asteroid. The 4.49 Ga ^{39}Ar–^{40}Ar age of Portales Valley (Pinault et al., 1999b) indicates that this impact event occurred $\sim$60 Ma after accretion of the asteroid.

4.3.3. The petrologic type of the target material

An important question is the mean petrologic type of the target material before the massive deposition of heat that resulted in the metal/silicate structure now preserved in Portales Valley. The two extreme possibilities are that the target was a primitive, type 3.0 chondrite possibly still retaining the inferred very high porosity of the first generation of nebular planetesimals, or that the target was already metamorphosed to the type-6 petrologic grade observed in clast E. If the porosity had been relatively high, this would have enhanced the $P \cdot \Delta V$ heating of the impact. However, because there is no correlation between porosity and petrologic type (Consolmagno et al., 1998), an assumed high porosity of the target does not uniquely define the petrologic type. It is likely that clast E will have undergone some

metamorphic recrystallization as a result of the energy deposited by the impact. Therefore, the target material was probably of a petrologic type less than 6. It could have been a porous H chondrite of relatively low petrologic type.

4.4. Related Meteorites

4.4.1. Netschaëvo

A meteorite that resembles Portales Valley is the Netschaëvo anomalous IIE iron. The available materials of this meteorite consists of ~25 vol.% angular, recrystallized, chondrule-bearing silicate clasts surrounded by swathing kamacite and dispersed in a metallic Fe–Ni host; the metal has a medium octahedrite structure with a kamacite bandwidth of 1.25 ± 0.35 mm (Buchwald, 1975; Bild and Wasson, 1977). The silicates show only very weak shock effects, i.e., S2 (Rubin, 1990), but there are curvilinear trails of tiny metal blebs within some silicate grains similar to those in Portales Valley. As in Portales Valley, troilite is mainly associated with the silicate clasts and occurs at metal–silicate boundaries, but is not associated with the metal host (Buchwald, 1975). Although the recovered Netschaëvo fragments contain a higher proportion of metal than Portales Valley, they are similar in containing angular silicate clasts that appear to have once fit together but are now separated a few millimeters by metal veins (e.g., Fig. 1238 of Buchwald, 1975). One significant difference between Netschaëvo and Portales Valley is that none of the chondritic fragments in Netschaëvo that we have examined are recognizably depleted in metal or enriched in sulfide.

Wasson and Wang (1986) modeled Netschaëvo and other IIE irons as having formed from impact melts near the surface of a chondritic asteroid. The Netschaëvo silicates were assumed to be annealed fragments of the country rock, but it seems possible that some are recrystallized fragments that were partly melted by impact. After its formation, Netschaëvo cooled slowly through ~500°C: fairly similar metallographic cooling rates were obtained for the metal matrix (1.4°C Ma^{-1}; Scott and Wasson, 1976) and for taenite grains in the silicate clasts (~3°C Ma^{-1}; Rubin, 1990).

Although it may have formed by processes that are in part analogous to those that formed Portales Valley, Netschaëvo probably did not form on the H-chondrite parent body: Its O-isotopic composition ($\delta^{17}O$ = 2.21‰; $\delta^{18}O$ = 3.53‰; $\Delta^{17}O$ = 0.37‰; Clayton et al., 1983) is distinctly lighter than that of H-group chondrites ($\delta^{17}O$ = 2.85 ± 0.15‰; $\delta^{18}O$ = 4.08 ± 0.22‰; $\Delta^{17}O$ = 0.72‰; Clayton et al., 1991); its equilibrated olivine composition is more reduced than that of H chondrites (Fa14.3 vs. Fa17.3–20.2; Rubin, 1990); and the siderophile element abundances in the silicate fragments are 60–100% greater than those in H chondrites (Bild and Wasson, 1977). Because these characteristics are those predicted by extrapolating OC trends to more reduced rocks, Bild and Wasson (1977) suggested that Netschaëvo is the first member of an ordinary chondrite group more reduced than H.

4.4.2. IIE irons and H chondrites

Three other meteorites (two IIE irons and a metal-rich H chondrite) may have formed in part in an analogous manner to Portales Valley. (1) Techado (IIE) contains a chondrule-free silicate inclusion of chondritic composition (Casanova et al., 1995). The inclusion is more reduced than typical H chondrites (Fa16.4 vs. Fa17.3–20.2 in H4-6 chondrites); it contains more (~26 wt.%) metal than mean H chondrites (18.6 wt.%), and is enriched in troilite (~10 wt.%) relative to mean H chondrites (5.3 wt.%; Dodd, 1981). If the Wasson and Wang (1986) model for the formation of IIE irons by impact melting near the surface of a chondritic parent body is correct, then the silicate inclusion in Techado may represent partly melted country rock. (2) Watson (IIE) contains a large (>30 cm^3) chondrule-free silicate inclusion with an igneous texture and H-chondrite-like mineral compositions (Olsen et al., 1994). The inclusion has clearly been melted; only small amounts of metal (0.3 wt.%) and troilite (0.9 wt.%) remain. It may have formed by complete melting of country rock; metal and sulfide lost from the silicate probably contributed to the metallic melt that formed the IIE host. (3) Y-791093 is a small meteorite (4.2 g) consisting of ~50 vol.% H6 chondrite clasts and ~50 vol.% of a metal–sulfide assemblage (Ikeda et al., 1997). However, the sample has been weathered to such an extent that all of the metal in the silicate clasts has been replaced by limonite. Although it may have formed in a similar manner to Techado and Watson, Y-791093 is too small and too weathered to model with confidence.

4.4.3. Blithfield

A meteorite that resembles Portales Valley in consisting of massive silicate-bearing, sulfide-poor, metal-rich regions surrounding large sulfide-rich, metal-poor silicate clasts is the Blithfield EL6 breccia. The Blithfield host consists of (in wt.%) 64% metal, 33% silicate, 2% phosphide, and 0.7% sulfide; the ~2 cm size clasts average 7% metal, 62% silicate, <0.1% phosphide, and 30% sulfide (Rubin, 1984). Blithfield contains no chondrules (Easton, 1983; Rubin, 1984) and, like other EL6 chondrites, exhibits only very weak (stage-S2) shock effects. Rubin et al. (1997) interpreted this meteorite as an annealed impact-melt breccia. Melting may have been sufficiently extensive to destroy all the chondrules and form coarse metal nodules and veins in the matrix; any chondrules that survived the melting episode may have been obliterated by intense recrystallization. The sulfide may have separated from metal in a manner similar to that proposed above for Portales Valley: some of the sulfide was present in a residual S-rich melt after much of the metallic liquid had crystallized. Additional sulfide in the clasts may have formed by reaction of metal in the clasts with an S_2-rich vapor formed during the impact event. Post-shock annealing may have caused recrystallization of clast-host boundaries, erasing such shock effects as highly undulose or mosaic extinction that may have been present in unmelted silicate grains.

5. CONCLUSIONS

It seems likely that Portales Valley is an annealed impact-melt breccia. The high abundance of metallic Cu in the silicates as well as the curvilinear trails of tiny metallic Fe–Ni blebs are characteristic of shocked and annealed chondrites. Some portions (e.g., clast E) appear to have experienced little or no melting and are essentially indistinguishable from normal H6 chondrites. Other regions (e.g., clasts A, D, and R) are finer grained, contain far fewer recognizable relict chondrules than

clast E, and show petrographic evidence of appreciable melting. We suggest that these experienced 20–40% melting.

Evidence that the metal was molten includes the general absence of entrained silicates, the three-dimensional interconnectedness of the metal, the occurrence of several rounded and scalloped silicate clasts (which appear to have been partly melted) surrounded by metal, and the composition of the metal which may reflect minor fractional crystallization. At the calculated liquidus temperature of the metal, we infer appreciable (≈40%) melting of H-chondrite silicates. However, because the mean temperature of the silicates was probably 100–300 K lower, they were most likely <30% molten.

Slow cooling of the rock is indicated by its Widmanstätten pattern, the multi-centimeter-size of the original taenite crystals, the metallographic cooling rate of 10 K Ma^{-1} through 500°C, the M-shaped compositional Ni profiles among taenite grains in the metal veins and silicate clasts, the Ni depletions at the surfaces of kamacite grains at the boundary with taenite and the occurrence of tetrataenite in the silicate clasts. Because curvilinear trails of opaque grains in most shocked chondrites are dominated by troilite, the essential absence of troilite in these trails in relict silicate grains in Portales Valley may indicate higher temperatures in Portales Valley (with most S in the vapor) than in chondrites that probably reached temperatures near the Fe–FeS eutectic (988°C) in which the curvilinear opaque trails are dominated by FeS. Annealing is also responsible for repairing shock damage of the olivine lattice, thereby lowering the apparent shock stage to S1.

It seems likely that Portales Valley formed on a large, low-density, porous asteroid where a high-energy impact caused variable degrees of crushing, heating, and melting followed by infall of wall rock, deep burial and slow cooling of the target material. Alternatively, it could have formed within a low-density, porous region of an asteroid with higher bulk density and lower global porosity. Portales Valley apparently formed from normal H-chondrite material. If we make the assumption that all H-chondrite samples in our meteorite collections originated on a single H-chondrite parent body, then some fraction of that body was of low density and high porosity.

Meteorites that are analogous to Portales Valley in some respects and thus may have formed by similar processes include the Netschaëvo IIE-an iron, the Techado and Watson IIE irons, and the EL6 Blithfield breccia.

Acknowledgments—We are most grateful to the following individuals who loaned or gave samples to us for study: D. Pitt, M. Cottingham, M. Killgore, E. R. D. Scott, A. J. Brearley, and D. W. Mittlefehldt. We thank E. R. D. Scott, J. N. Grossman, H. J. Melosh, D. A. Kring, A. J. Brearley, D. D. Bogard, M. Killgore, A. Ruzicka, C. R. Chapman, M. J. Gaffey, and W. F. Bottke for informative discussions and R. N. Clayton for the use of unpublished data. We are grateful to J. Richardson for technical assistance. We thank R. Ketcham and M. Colbert for participation in collecting the HRXCT data, and C. Denison for assistance in visualization and image analysis. Reviews by A. Ruzicka, G. J. Taylor, and C. R. Chapman were helpful in improving the paper. This work was supported in part by NASA Grant No. NAG5-4766 (A. E. Rubin) and by NSF Grant No. EAR-9816020 (W. D. Carlson and R. A. Ketcham).

REFERENCES

Afiattalab F. and Wasson J. T. (1980) Composition of the metal phases in ordinary chondrites: Implications regarding classification and metamorphism. *Geochim. Cosmochim. Acta* **44,** 431–446.

Ashworth J. R. (1985) Transmission electron microscopy of L-group chondrites. 1. Natural shock effects. *Earth Planet. Sci. Lett.* **73,** 17–32.

Bauer J. F. (1979) Experimental shock metamorphism of mono- and polycrystalline olivine: A comparative study. *Proc. Lunar Planet. Sci. Conf.* **10,** 2573–2596.

Begemann F. and Wlotzka F. (1969) Shock induced thermal metamorphism and mechanical deformations in the Ramsdorf chondrite. *Geochim. Cosmochim. Acta* **33,** 1351–1370.

Bennett M. E. and McSween H. Y. (1996) Shock features in iron-nickel metal and troilite of L-group ordinary chondrites. *Meteorit. Planet. Sci.* **31,** 255–264.

Benoit P. H., Akridge G., and Sears D. W. G. (1998) Size sorting of metal, sulfide, and chondrules in Sharps (H3.4). *Lunar Planet. Sci.* **29,** abstract #1457. Lunar and Planetary Institute.

Bild R. W. and Wasson J. T. (1977) Netschaëvo: A new class of chondrite meteorite. *Science* **197,** 58–62.

Bottke W. F., Richardson D. C., Michel P., and Love S. G. (1999) 1620 Geographos and 433 Eros: Shaped by planetary tides. *Astron. J.* **117,** 1921–1928.

Brandes E. A. and Brook G. B. (1998) *Smithells Metals Reference Book*, Seventh ed., Butterworth-Heinemann.

Brearley A. J. and Jones R. H. (1998) Chondritic meteorites. In *Planetary Materials, Reviews in Mineralogy* (ed. J. J. Papike), Vol. 36, pp. 3-1–3-398. Mineralogical Society of America.

Brearley A. J., Casanova I., Miller M. L., and Keil K. (1991) Mineralogy and possible origin of an unusual Cr-rich inclusion in the Los Martinez (L6) chondrite. *Meteoritics* **26,** 287–300.

Buchwald V. F. (1975) *Handbook of Iron Meteorites*. University of California Press.

Cameron A. G. W., Benz W., and Wasson J. T. (1990) Heating during asteroidal collisions (abstract). *Lunar Planet. Sci.* **21,** 155–156.

Carlson W. D. and Dension C. (1992) Mechanisms of porphyroblast crystallization: Results from high-resolution computed x-ray tomography. *Science* **257,** 1236–1239.

Casanova I., Graf T., and Marti K. (1995) Discovery of an unmelted H-chondrite inclusion in an iron meteorite. *Science* **268,** 540–542.

Cheng A. F. and Barnouin-Jha O. S. (1999) Giant craters on Mathilde. *Icarus* **140,** 34–48.

Chou C.-L., Baedecker P. A., and Wasson J. T. (1973) Distribution of Ni, Ga, Ge and Ir between metal and silicate portions of H-group chondrites. *Geochim. Cosmochim. Acta* **37,** 2159–2171.

Clayton R. N., Mayeda T. K., Olsen E. J., and Prinz M. (1983) Oxygen isotope relationships in iron meteorites. *Earth Planet. Sci. Lett.* **65,** 229–232.

Clayton R. N., Mayeda T. K., Goswami J. N., and Olsen E. J. (1991) Oxygen isotope studies of ordinary chondrites. *Geochim. Cosmochim. Acta* **55,** 2317–2337.

Consolmagno G. J., Britt D. T., and Stoll C. P. (1998) The porosities of ordinary chondrites: Models and interpretation. *Meteorit. Planet. Sci.* **33,** 1221–1229.

Crabb J. and Schultz L. (1981) Cosmic-ray exposure ages of the ordinary chondrites and their significance for parent body stratigraphy. *Geochim. Cosmochim. Acta* **45,** 2151–2160.

Davis D. R., Chapman C. R., Greenberg R., and Weidenschilling S. J. (1979) Collisional evolution of asteroids: Populations, rotations, and velocities. In: *Asteroids* (ed. T. Gehrels), pp. 528–557, University of Arizona Press.

Dodd R. T. (1981) *Meteorites—A Petrologic-Chemical Synthesis*. Cambridge University Press.

Dodd R. T. and Jarosewich E. (1982) The compositions of incipient shock melts in L6 chondrites. *Earth Planet. Sci. Lett.* **59,** 355–363.

Easton A. J. (1983) Grain-size distribution and morphology of metal in E-chondrites. *Meteoritics* **18,** 19–27.

Fish R. A., Goles G. G., and Anders E. (1960) The record in the meteorites. III. On the development of meteorites in asteroidal bodies. *Astrophys. J.* **132,** 243–258.

Gomes C. B. and Keil K. (1980) *Brazilian Stone Meteorites*. University of New Mexico.

Graf T. and Marti K. (1995) Collisional history of H chondrites. *J. Geophys. Res.* **100,** 21,247–21,263.

Graham A. L., Bevan A. W. R., and Hutchison R. (1985) *Catalogue of Meteorites*. University of Arizona Press.

Grimm R. E. and McSween H. (1993) Heliocentric zoning of the asteroid belt by 26-Al heating. *Science* **259,** 653–655.

Harris A. W. (1996) The rotation rates of very small asteroids: Evidence for "rubble pile" structure (abstract). *Lunar Planet. Sci.* **27,** 493–494.

Hartmann W. K. (1979) Diverse puzzling asteroids and a possible unified explanation. In *Asteroids* (ed. T. Gehrels), pp. 466–479. University of Arizona Press.

Herbert F., Sonett C. P., and Gaffey M. J. (1991) Protoplanetary thermal metamorphism: The hypothesis of electromagnetic induction in the protosolar wind. In *The Sun in Time* (ed. C. P. Sonett, M. S. Giampapa, and M. S. Matthews), pp. 710–739. University of Arizona Press.

Heymann D. (1967) On the origin of hypersthene chondrites: Ages and shock effects of black chondrites. *Icarus* **6,** 189–221.

Housen K. R. and Holsapple K. A. (1999) Impact cratering on porous low-density bodies. *Lunar Planet Sci.* **30,** abstract #1228. Lunar and Planetary Institute.

Ikeda Y., Yamamoto T., Kojima H., Imae N., Kong P., Ebihara M., and Prinz M. (1997) Yamato-791093, a metal-sulfide-enriched H-group chondritic meteorite transitional to primitive IIE irons with silicate inclusions. *Antarct. Met. Res.* **10,** 335–353.

Jurewicz A. J. G., Jones J. H., Weber E. T., and Mittlefehldt D. W. (1993) Partial melting of ordinary chondrites: Lost City (H) and St. Severin (LL). *Lunar Planet. Sci.* **24,** 739–740.

Kallemeyn G. W., Rubin A. E., Wang D., and Wasson J. T. (1989) Ordinary chondrites: Bulk compositions, classification, lithophile-element fractionations, and composition-petrographic type relationships. *Geochim. Cosmochim. Acta* **53,** 2747–2767.

Keil K. (1962) Quantitativ=erzmikroskopische Integrationsanalyse der Chondrite. *Chem. Erde* **22,** 281–348.

Keil K., Kirchner E., Gomes C. B., and Nelen J. (1977) Studies of Brazilian meteorites. V. Evidence for shock metamorphism in the Paranaiba, Mato Grosso, chondrite. *Rev. Brasil. Geo.* **7,** 256–268.

Kring D. A., Hill D. H., Gleason J. D., Britt D. T., Consolmagno G. J., Farmer M., Wilson S., and Haag R. (1999) Portales Valley: A meteoritic sample of the brecciated and metal-veined floor of an impact crater on an H-chondrite asteroid. *Meteorit. Planet. Sci.* **34,** 663–669.

Krot A. N. and Rubin A. E. (1993) Chromite-rich mafic silicate chondrules in ordinary chondrites: Formation by impact melting (abstract). *Lunar Planet. Sci.* **24,** 827–828.

Lauretta D. S., Lodders K., Fegley B., and Kremser D. T. (1997) The origin of sulfide-rimmed metal grains in ordinary chondrites. *Earth Planet. Sci. Lett.* **151,** 289–301.

Lee T., Papanastassiou D. A., and Wasserburg G. J. (1976) Demonstration of ^{26}Mg excess in Allende and evidence for ^{26}Al. *Geophys. Res. Lett.* **3,** 109–112.

McHone J. F., Killgore M., and Killgore E. (1999) Portales Valley, New Mexico fall of 13 June 1998: Anomalous fragment distribution and composition. *Lunar Planet. Sci.* **30,** abstract #1964. Lunar and Planetary Institute.

Melosh H. J. (1989) *Impact Cratering: A Geologic Process*. Oxford University Press.

Murrell M. T. and Burnett D. S. (1983) The behavior of actinides, phosphorus, and rare earth elements during chondrite metamorphism. *Geochim. Cosmochim. Acta* **47,** 1999–2014.

Olsen E., Davis A., Clarke R. S., Schultz L., Weber H. W., Clayton R., Mayeda T., Jarosewich E., Sylvester P., Grossman L., Wang M.-S., Lipschutz M. E., Steele I. M., and Schwade J. (1994) Watson: A new link in the IIE iron chain. *Meteoritics* **29,** 200–213.

Ostro S. J., Hudson R. S., Jurgens R. F., Rosema K. D., Campbell D. B., Yeomans D. K., Chandler J. F., Giorgini J. D., Winkler R., Rose R., Howard S. D., Slade M. A., Perillat P., and Shapiro I. I. (1995) Radar images of asteroid 4179 Toutatis. *Science* **270,** 80–83.

Pinault L. J., Scott E. R. D., Bogard D. D., and Keil K. (1999a) Extraordinary properties of the metal-veined, H6 Portales Valley chondrite: Evidence for internal heating versus shock-melting origins. *Lunar Planet. Sci.* **30,** abstract #2048, Lunar and Planetary Institute.

Pinault L. J., Scott E. R. D., Bogard D. D., and Keil K. (1999b) Portales Valley, A metal-veined H6 chondrite with evidence of internally-generated partial melting of Fe-Ni-S (abstract). *Antarct. Met.* **24,** 157–159. National Institute Polar Research.

Rambaldi E. R. (1977) Trace element content of metals from H- and LL-group chondrites. *Earth Planet. Sci. Lett.* **36,** 347–358.

Rambaldi E. R. and Cendales M. (1979) Moderately volatile siderophiles in ordinary chondrites. *Earth Planet. Sci. Lett.* **44,** 397–408.

Ramdohr P. (1967) Chromite and chromite chondrules in meteorites. I. *Geochim. Cosmochim. Acta* **31,** 1961–1967.

Rasmussen K. L., Ulff-Møller F., and Haack H. (1995) The thermal evolution of IVA iron meteorites: Evidence from metallographic cooling rates. *Geochim. Cosmochim. Acta* **59,** 3049–3059.

Rinehart J. S. (1968) Intense destructive stresses resulting from stress wave interactions. In *Shock Metamorphism of Natural Materials* (eds. B. M. French and N. M. Short). Mono Book Corp.

Rubin A. E. (1984) The Blithfield meteorite and the origin of sulfide-rich, metal-poor clasts and inclusions in brecciated enstatite chondrites. *Earth Planet. Sci. Lett.* **67,** 273–283.

Rubin A. E. (1985) Impact melt products of chondritic material. *Rev. Geophys.* **23,** 277–300.

Rubin A. E. (1990) Kamacite and olivine in ordinary chondrites: Intergroup and intragroup relationships. *Geochim. Cosmochim. Acta* **54,** 1217–1232.

Rubin A. E. (1992) A shock-metamorphic model for silicate darkening and compositionally variable plagioclase in CK and ordinary chondrites. *Geochim. Cosmochim. Acta* **56,** 1705–1714.

Rubin A. E. (1994) Metallic copper in ordinary chondrites. *Meteoritics* **29,** 93–98.

Rubin A. E. (1995a) Petrologic evidence for collisional heating of chondritic asteroids. *Icarus* **113,** 156–167.

Rubin A. E. (1995b) Fractionation of refractory siderophile elements in metal from the Rose City meteorite. *Meteoritics* **30,** 412–417.

Rubin A. E. (1999) Formation of large metal nodules in ordinary chondrites. *J. Geophys. Res.* **104,** 30,799–30,804.

Rubin A. E. and Arnold S. (2000) The Smyer H-chondrite impact-melt breccia: Evidence for sulfur vaporization during shock. *Meteorit. Planet. Sci.* **35,** A138–A139.

Rubin A. E. and Ulff-Møller F. (1999) The Portales Valley meteorite breccia: Evidence for impact-induced metamorphism of an ordinary chondrite. *Lunar Planet. Sci.* **30,** abstract #1125. Lunar and Planetary Institute.

Rubin A. E., Scott E. R. D., and Keil K. (1997) Shock metamorphism of enstatite chondrites. *Geochim. Cosmochim. Acta* **61,** 847–858.

Ruzicka A., Snyder G. A., Prinz M., and Taylor L. A. (1999a) Portales Valley: A new metal-phosphate-rich meteorite with affinities to Netschaëvo and H-group chondrites. *Lunar Planet. Sci.* **30,** abstract #1645. Lunar and Planetary Institute.

Ruzicka A., Bennett M. E., Patchen A. D., Snyder G. A., and Taylor L. A. (1999b) Widmanstätten texture in the Portales Valley meteorite: Slow (but not unusually slow) cooling at low temperatures. *Lunar Planet. Sci.* **30,** abstract #1616. Lunar and Planetary Institute.

Ruzicka A., McHone J. F., and Killgore M. (2000) Portales Valley: Discovery of a large graphite nodule (abstract). *Meteorit. Planet. Sci.* **35,** A140.

Scott E. R. D. and Pinault L. J. (1999) Partial melting and incipient segregation of troilite and metal in winonaites, acapulcoites, IAB and IIE irons, and fine-grained H6 chondrites. *Lunar Planet. Sci.* **30,** abstract #1507. Lunar and Planetary Institute.

Scott E. R. D. and Wasson J. T. (1976) Chemical classification of iron meteorites—VII. Groups IC, IIE, IIIF and 97 other irons. *Geochim. Cosmochim. Acta* **40,** 103–115.

Smith B. A. and Goldstein J. I. (1977) The metallic microstructures and thermal histories of severely reheated chondrites. *Geochim. Cosmochim. Acta* **41,** 1061–1072.

Sonett C. P., Colburn D. S., Schwartz K., and Keil K. (1970) The melting of asteroidal-sized bodies by unipolar dynamo induction from a primordial T Tauri sun. *Astrophys. Space Phys.* **7,** 446–488.

Stöffler D., Keil K., and Scott E. R. D. (1991) Shock metamorphism of ordinary chondrites. *Geochim. Cosmochim. Acta* **55,** 3845–3867.

Ulff-Møller F., Choi B.-G., Rubin A. E., Tran J., and Wasson J. T. (1998) Paucity of sulfide in a large slab of Esquel: New perspectives on pallasite formation. *Met. Planet. Sci.* **33,** 331–227.

Urey H. C. (1955) The cosmic abundances of potassium, uranium, and

thorium and the heat balances of the Earth, the Moon, and Mars. *Proc. Natl. Acad. Sci.* **41,** 127–144.

Van Schmus W. R. and Ribbe P. H. (1968) The composition and structural state of feldspar from chondritic meteorites. *Geochim. Cosmochim. Acta* **32,** 1327–1342.

Van Schmus W. R. and Wood J. A. (1967) A chemical-petrologic classification for the chondritic meteorites. *Geochim. Cosmochim. Acta* **31,** 747–765.

Veverka J., Thomas P., Harch A., Clark B., Bell III J. F., Carcich B., Joseph J., Chapman C., Merline W., Robinson M., Malin M., A. M. L., Murchie S., Hawkins III S. E., Farquhar R., Izenberg N., and A. C. (1997) NEAR's flyby of 253 Mathilde: Images of a C asteroid. *Science* **278,** 2109–2114.

Voshage H. (1967) Bestrahlungsalter und Herkunft der Eisenmeteorite. *Z. Naturforsch.* **22a,** 477–506.

Wasson J. T. and Richardson J. W. (2001) Fractionation trends among IVA iron meteorites: Contrasts with IIIAB trends. *Geochim. Cosmochim. Acta,* in press.

Wasson J. T. and Wang J. (1986) A nonmagmatic origin of group IIE iron meteorites. *Geochim. Cosmochim. Acta* **50,** 725–732.

Wasson J. T., Rubin A. E., and Benz W. (1987) Heating of primitive, asteroid-size bodies by large impacts. *Meteoritics* **22,** 525–526.

Wasson J. T., Ouyang X., Wang J., and Jerde E. (1989) Chemical classification of iron meteorites: XI. Multi-element studies of 38 new irons and the high abundance of ungrouped irons from Antarctica. *Geochim. Cosmochim. Acta* **53,** 735–744.

Widom E., Rubin A. E., and Wasson J. T. (1986) Composition and formation of metal nodules and veins in ordinary chondrules. *Geochim. Cosmochim. Acta* **50,** 1989–1995.

Yeomans D. K., Barriot J.-P., Dunham D. W., Farquhar R. W., Giorgini J. D., Helfrich C. E., Konopliv A. S., McAdams J. V., Miller J. K., Owen, Jr. W. M., Scheeres D. J., Synnott S. P., and Williams B. G. (1997) Estimating the mass of asteroid 253 Mathilde from tracking data during the NEAR flyby. *Science* **278,** 2106–2109.